University of Tartu
Faculty of Science and Technology
Institute of Ecology and Earth Sciences
Department of Geology

Master's thesis in geology (30 ECTS)

Insight into the sulfur cycle in the Baltic Sea surface sediments based on sulfur isotope records

Krete Roopõld

Supervisors: Martin Liira
Kärt Paiste

Tartu 2025

Insight into the sulfur cycle in the Baltic Sea surface sediments based on sulfur isotope records

This thesis explores the sufur cycle in the surface sediments of the Northern Baltic Sea, focusing on the isotopic composition of reduced sulfur. Additionally, the work includes setting up and validating an extraction line for acid volatile sulfide (AVS) and chromium reducible sufur (CRS) at the University of Tartu. The extraction line proved effective for extracting sulfur species for isotope analysis but requires further improvements for achieving quantitative recoveries. Isotopic analyses of AVS and pyrite sulfur from three stations revealed significant differences in $\delta^{34}S$ values despite similar sediment composition. This study suggests that the differences are linked to depositional conditions such as water depth, sedimentation rate, and redox state that create variabilities in system openness. The findings highlight the complexity of sulfur cycling and the importance of integrating depositional context and geochemical data to interpret isotopic signals in marine sediments.

Keywords: Marine sediments, sulfur cycle, Baltic Sea, sulfur isotopes, pyrite
CERCS code: P420 petrology, mineralogy, geochemistry

Läänemere merepõhja pindmiste setete väävliringest väävli isotoopsignaalide põhjal

Käesolev magistritöö uurib väävliringet Läänemere põhjaosa pindmistes setetes, keskendudes redutseeritud väävli isotoopkoostisele. Töö osaks on ka laboratoorse ekstraheerimisliini üles seadmine ja valideerimine happes lahustuva sulfiidi (AVS) ja kroomiga redutseeritava väävli (CRS) eraldamiseks Tartu Ülikoolis. Ekstraheerimisliin osutus tõhusaks, kui eesmärgiks on väävliühendite isotoopanalüüs, kuid vajab edasisi täiendusi kvantitatiivseteks analüüsideks. Uuritud jaamades leiduva AVS-i ja püriidi väävli isotoopkoostised näitasid märkimisväärseid erinevusi hoolimata sarnasest settetüübist. Uuring viitab sellele, et varieeruvus on seotud settekeskkonna tingimustega nagu veesügavus, settimiskiirus ja põhjakihi hapnikusisaldus, mis mõjutavad süsteemi avatust. Tulemused rõhutavad väävliringe keerukust ning settekeskkonna ja geokeemiliste andmete integreerimise olulisust isotoopsignaalide interpreteerimisel.

Märksõnad: Merepõhja setted, väävliringe, Läänemeri, väävli isotoobid, püriit
CERCS kood: P420 petroloogia, mineraloogia, geokeemia

Table of Contents

1. Introduction

The sulfur cycle is an important component of Earth's biogeochemical systems, regulating the transformation of sulfur between its various species. By influencing the carbon cycling and the redox state of the oceans, it has long-term implications for the climate. It plays a crucial role in organic matter degradation, metal mobility, and long-term sequestration of sulfur in the form of sulfide minerals (Jørgensen & Kasten, 2006). Among these, pyrite (FeS_2) formation is of particular interest due to its implications for both modern environmental processes and the interpretation of ancient sedimentary records (Fike et al., 2015).

The Baltic Sea, a semi-enclosed brackish basin in Northern Europe, presents a unique natural laboratory for studying sulfur cycling under varying redox conditions. The variations in organic matter input, sulfate availability, and bottom water oxygenation govern the transformation and burial of sulfur species, making this region especially relevant for understanding the controls on the sulfur cycle and sulfur isotope fractionation (Jørgensen et al., 2019a).

Despite the importance of sulfur cycling in the Baltic Sea, detailed studies on the isotopic composition of sedimentary sulfur species and their environmental drivers remain limited in the region. Furthermore, the technical capacity for sulfur speciation has been lacking in many laboratories. This thesis addresses these gaps by establishing a sulfur extraction line for acid volatile sulfide (AVS) and chromium reducible sulfur (CRS) at the University of Tartu and applying it to sediment cores collected from the Estonian Baltic Sea.

This thesis aims to (1) set up an extraction line for AVS and CRS at the University of Tartu and validate the extraction line efficiency with reference materials and (2) investigate the sulfur cycle in the Estonian Baltic Sea sediments by examining both spatial and vertical variations in mineralogical, chemical, and sulfur isotope compositions. The central hypotheses of this study are that (1) AVS and CRS extractions are suitable methods to analyse sulfur cycle in the Baltic Sea sediments and (2) the isotope signals from reduced sulfur in sediments are influenced by the depositional environment, particularly by factors such as water depth, sedimentation rate and, organic matter availability.

2. The sulfur cycle and the Baltic Sea

2.1 The sulfur cycle

In natural environments, sulfur (S) occurs in different forms with oxidation states between -2 to +6 (Jørgensen & Kasten, 2006). The most common sulfur species found in nature are sulfate (SO_4^{2-}), sulfide (S^{2-} or S^{1-}), and elemental sulfur (S^0). Sulfate is the oxidized and water-soluble form, while sulfide is the reduced form found in low-oxygen environments. Elemental sulfur is the intermediate. These sulfur species are interconnected through the sulfur cycle, where biological and geological processes facilitate the conversion of sulfur between them (Jørgensen & Kasten, 2006).

The sulfate concentration in ocean water is about 28.7 mM, making the ocean one of the largest sulfur reservoirs, with about 1.3 x 10^9 Tg (teragram = 10^{12} g) of sulfur (Vairavamurthy et al., 1995). Most of the dissolved sulfur originates from weathered continental rocks and is carried to the oceans by rivers. Atmospheric inputs, including recycled sulfur in seaspray, volcanic gases, and anthropogenic emissions, are considered of lesser significance relative to the riverine input (Jørgensen & Kasten, 2006; Vairavamurthy et al., 1995).

The main sink for oceanic sulfur is the marine sediments. Sulfate in the ocean water can be transferred and captured in the sediments through three major processes: (1) sulfate reduction to hydrogen sulfide (H_2S) and formation of sulfide minerals, most importantly Fe-sulfides and mainly as pyrite (FeS_2), (2) incorporation of sulfur into organosulfur compounds, and (3) formation of sulfate minerals in sediments (Vairavamurthy et al., 1995). Vairavamurthy et al., (1995) suggests that the latter mechanism is dominant in very specific geologic settings (i.e., evaporitic basins) and is of minor importance in today's oceans.

Broadly, the global sulfur cycle incorporates the weathering of sulfur-containing rocks, transport of sulfate into the oceans, burial of sulfur as sulfides, organic sulfur or sulfate salts, and uplift of seafloor deposits, bringing the sulfur back on land (Canfield et al., 2005).

Sulfur cycling in marine sediments plays a critical role in global biogeochemical processes, particularly in the decomposition of organic matter under anoxic conditions through organoclastic sulfate reduction (Jørgensen & Kasten, 2006). This process not only drives the transformation of organic carbon into carbon dioxide but also produces hydrogen sulfide,

which interacts with metal ions to form insoluble metal sulfides, thereby influencing metal bioavailability and toxicity (Jørgensen & Kasten, 2006). Additionally, the burial of reduced sulfur compounds such as pyrite contributes to the long-term regulation of oceanic and atmospheric oxygen levels (Fike et al., 2015). Sulfur cycling is thus tightly linked to carbon cycling, nutrient dynamics, and climate regulation, while also supporting unique chemosynthetic ecosystems in marine environments. The rest of this overview focuses on the processes occurring in the seafloor sediments, particularly sulfate reduction, sulfide oxidation, sulfur disproportionation, and Fe-sulfide formation, summarized in figure 1.

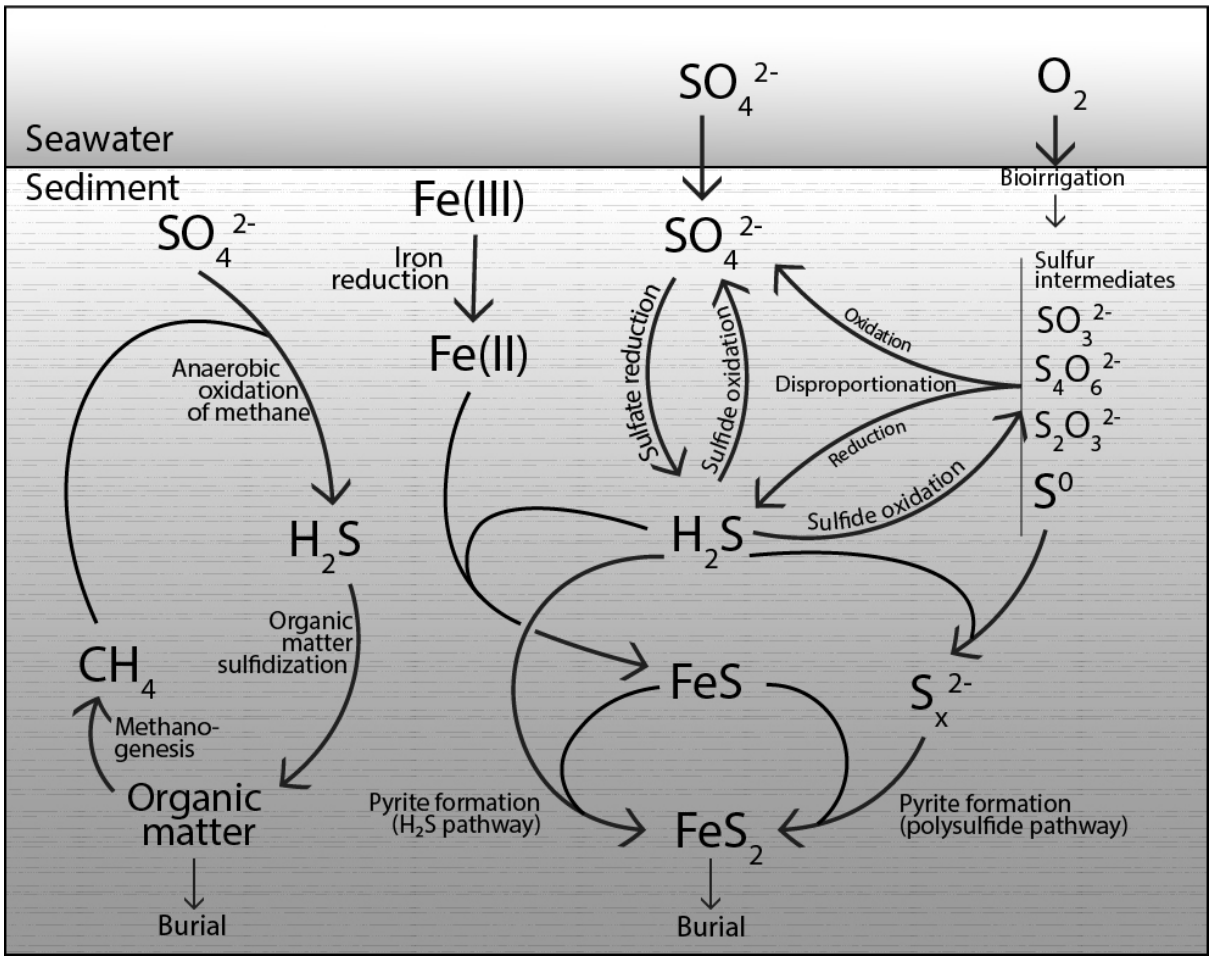

Figure 1. The sulfur cycle in the marine sediments (modified from Jørgensen, 2021).

2.1.1 Organic matter degradation, sulfate reduction, and AOM

The most important biogeochemical processes in marine sediments are associated with organic matter degradation. Most of the organic matter is produced in the photic zone of the water column through photosynthesis (Vairavamurthy et al., 1995). Additionally, a small portion of the organic matter in the marine environments is of terrestrial origin, delivered through riverine run-off and airborne particulates (Rullkötter, 2006). Upon the demise of marine organisms, the organic matter sinks and begins to decompose back into CO_2 and nutrients. This oxidation process starts in the water column and continues in the sediments once it has settled on the seafloor (Rullkötter, 2006).

The degradation and mineralization processes are mediated by microorganisms that harness the energy released from the oxidation of organic matter. These processes consume various electron acceptors, particularly oxygen (O_2), nitrate (NO_3^-), Fe^{3+}, Mn^{4+}, and sulfate (SO_4^{2-}), which are gradually depleted in the sediments (Froelich et al., 1979; Schulz, 2006). Since respiration by oxygen is energetically most favourable, oxygen is consumed first (Froelich et al., 1979; Jørgensen & Kasten, 2006). Subsequently, other oxidants are utilized in the order of their energetic efficiency. In the absence of any oxidants, organic matter continues to degrade via methanogenesis. The sequential utilization of different electron acceptors gives rise to vertical geochemical zonation within the sediment pore water environment (figure 2). Apart from energetic favourability, the ordering and rate of the electron donor consumption depend on the genetic abilities of the local microbial communities and the reaction rates of each metabolic process (Fike et al., 2015).

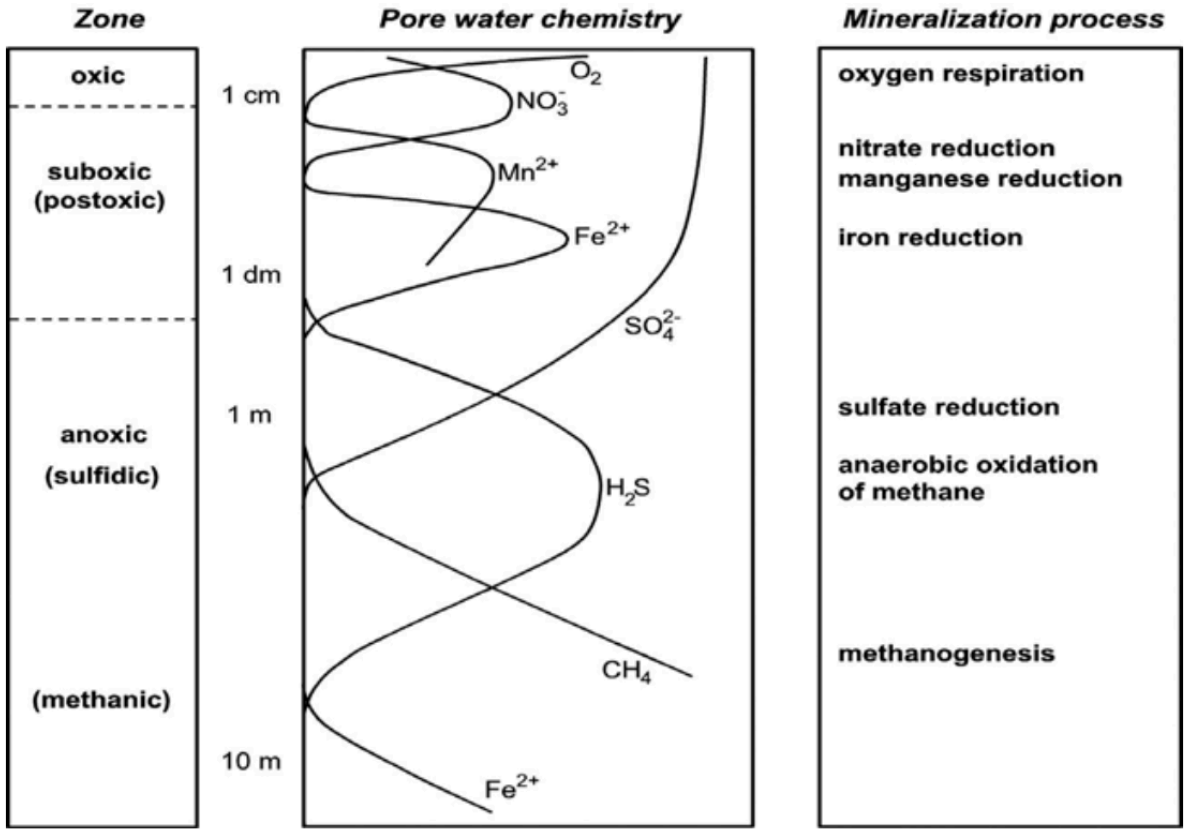

Figure 2. Biogeochemical zonation in marine sediments (from Jørgensen & Kasten, 2006).

The oxidation of organic matter which utilizes sulfate as the oxidant is called sulfate reduction (SR). In actuality, there are two mechanisms for how sulfate is reduced: 1) assimilatory sulfate reduction, where organisms use energy to reduce sulfate and produce sulfur-containing compounds essential for physiological functions, and 2) dissimilatory sulfate reduction, where organisms gain energy from reducing sulfate to hydrogen sulfide (Canfield et al., 2005). However, only the latter has an important role in organic matter mineralization and hydrogen sulfide production in marine sediments (Jørgensen & Kasten, 2006) and is therefore considered equivalent to the notion of "sulfate reduction" in this study. Dissimilatory sulfate reduction is described by the following net chemical equation:

$$2\,[CH_2O] + SO_4^{2-} \rightarrow 2\,HCO_3^- + H_2S$$

where $[CH_2O]$ represents the organic matter (Jørgensen & Kasten, 2006).

Sulfate reduction is believed to play a significant role in total organic matter mineralization, especially in near-shore areas with high sedimentation rates and lower water depths (Jørgensen,

1982). Sulfate reduction is estimated to be responsible for the oxidation of 77 Tmol of organic carbon per year, which is about a third of organic carbon mineralized in the seabed globally (Jørgensen, 2021; Jørgensen et al., 2024). About 80% of the global sulfate reduction occurs on the continental shelf (Egger et al., 2018).

Sulfate reduction is the main pathway for organic matter mineralization in the anoxic zone before sulfate is depleted, i.e., the sulfate reduction zone (see figure 2). The depth of the anoxic zone depends on various factors, such as oxygen content in the overlying water, bioturbation intensity, and, most importantly, organic matter sedimentation rates. In shallower waters with high organic matter sedimentation rates, the sulfate reduction zone may begin in the first cm-s below the seafloor, but in the deep sea, where organic matter sedimentation rate is low, it can start in the scale of meters below the seafloor (Jørgensen & Kasten, 2006). In specific parts of the ocean, oxygen may not reach depletion in the sediments, completely inhibiting sulfate reduction (D'Hondt et al., 2015; Røy et al., 2012).

The sulfate reduction rate is controlled by several factors, including the oxygenation of the environment, the availability of sulfate, the availability of electron donor (organic matter), and temperature (Canfield et al., 2005). Most sulfate-reducing microorganisms function in an anoxic environment. However, sulfate reduction has also been detected in suboxic and oxic zones, but there, the produced H_2S is rapidly reoxidized back to SO_4^{2-}, rendering the process undetectable in pore water sulfate profiles (Jørgensen & Bak, 1991). Sulfate must be available; when the concentration is low, sulfate is rapidly depleted leading to low overall intensity of sulfate reduction (Canfield et al., 2005). Bioturbation can enhance sulfate availability in the sediment. The concentration and degradability of organic matter present in the sediments also correlate with sulfate reduction rates (Canfield et al., 2005). For example, in large parts of the ocean, organic matter concentration is exceptionally low and sulfate never reaches depetion (Egger et al., 2018). Sulfate reduction rates typically increase with temperature and are subject to seasonal variations (Canfield et al., 2005).

When sulfate has been largely depleted from the pore water, methanogenesis is the main pathway for organic matter degradation. Egger et al., 2018 estimated that globally about 3–4% of carbon that reaches the seafloor is turned into methane. Most of the methane diffuses into the sulfate zone, where it is oxidized by sulfate. This process is called anaerobic oxidation of methane (AOM) and is characterized by the following equation (Jørgensen & Kasten, 2006):

$$CH_4 + SO_4^{2-} \rightarrow 2\ HCO_3^- + HS^- + H_2O$$

The narrow zone at the base of the sulfate zone where AOM occurs is called the sulfate-methane transition zone (SMTZ). In some settings, AOM can account for the consumption of all the sulfate that diffuses into the SMTZ from the sediment surface (Niewöhner et al., 1998).

2.1.2 Sulfide oxidation and disproportionation

It is estimated that over 90% of the hydrogen sulfide produced during sulfate reduction is oxidized back to sulfate (Jørgensen, 1982). This process can be inorganic or mediated by sulfide-oxidizing microorganisms (Canfield et al., 2005). Both pathways can be significant, but the quantitative controls are not fully understood (Canfield et al., 2005). Sulfide oxidation typically occurs close to the sediment surface, within oxic and suboxic zones. In the suboxic zone, the oxidants are Fe and Mn oxides, as well as nitrate, but the former are considered dominant. In the oxic zone, oxygen is the most effective oxidant.

Sulfide can be directly oxidized to sulfate but sulfide oxidation can also be partial, producing sulfur species with intermediate valences. These include polysulfide (S_x^{-2}), elemental sulfur (S_8), thiosulfate ($S_2O_3^{2-}$), tetrathionate ($S_2O_6^{2-}$), and sulfite (SO_3^{2-}) (Jørgensen et al., 2019a). These species can serve as electron acceptors during reduction and as donors during oxidation. The reactions involving sulfur intermediates lead to sulfur disproportionation (Fike et al., 2015).

The potential for sulfur disproportionation in marine sediments is considered high. Biologically mediated disproportionation reactions include the following: (Canfield et al., 2005)

$$4H_2O + 4S^0 \rightarrow 3H_2S + SO_4^{2-} + 2H^+$$

$$4SO_3^{2-} + 2H^+ \rightarrow 2H^+ \rightarrow H_2S + SO_4^{2-}$$

$$S_2O_3^{2-} + H_2O \rightarrow H_2S + SO_4^{2-}$$

$$4S^0 + 3H_2O \rightarrow H_2S + S_2O_3^{2-} + 2H^+$$

2.1.3 Pyrite formation

Approximately 90% of the sulfide produced during sulfate reduction is oxidized back to sulfate (Jørgensen, 1982). The remaining is transformed into sulfide minerals (mainly pyrite), which is the primary mechanism for sulfur burial (Jørgensen et al., 2019a). Simply put, pyrite forms through the oxidation of hydrogen sulfide by ferric iron (Fe^{3+}) minerals in the sediment. Through this reaction, ferrous iron (Fe^{2+}) along with elemental sulfur and polysulfides are formed. Reduced iron (Fe^{2+}) can then react with S^{2-} to form iron monosulfide FeS (Rickard & Luther, 2007). The iron monosulfide (FeS) formed in sediments is the brownish-black mineral mackinawite, although it is sometimes referred to as amorphous FeS because it commonly forms as nanoscale crystals that produce a broad peak in X-ray diffraction analysis (Rickard & Luther, 2007).

It has been argued that pyrite eventually forms from dissolved FeS through two main pathways: the H_2S pathway and the polysulfide pathway (Jørgensen et al., 2019a; Rickard & Luther, 1997, 2007).

$$FeS + H_2S \rightarrow FeS_2 + H_2 \quad (H_2S \text{ pathway})$$

$$FeS + S_x^{2-} \rightarrow FeS_2 + S_{x-1}^{2-} \quad (\text{Polysulfide pathway})$$

These reactions occur inorganically, but microorganisms may affect pyrite formation kinetics as catalysts (Canfield et al., 1998; Rickard, 2012).

The two most common textures for sedimentary pyrite are single crystals and framboids and the occurrence of these depends on the crystal formation kinetics (Rickard, 2012). Pyrite crystal formation consists of two processes: nucleation and crystal growth. While single crystals form with limited nucleation and continuous crystal growth at low supersaturations, framboids require high nucleation rates, which require extreme supersaturations (Rickard, 2012). Foreign objects can serve as nucleation centres, making heterogenous nucleation a more plausible mechanism in natural environments, as it requires lower supersaturations (Wang & Morse, 1996). After nucleation, the growth of pyrite crystals involves a reaction between Fe^{2+} and S_2^{2-} and does not need FeS as an intermediate (Rickard & Luther, 2007)

Pyrite framboids, which consist of cubic or octahedral microcrystals, are commonly found in marine sediments (Rickard, 2012). Pyrite framboids can capture snapshots of pore water chemical composition, as they can form very quickly, within hours or days (Rickard, 2019), making them ideal targets for investigating S cycling in sediments. However, they can be easily overgrown by subsequent pyrite generation or recrystallize over time (e.g., Fike et al., 2015; Paiste et al., 2024). Depth in the sediment profile will have a significant influence on their morphology and sulfur isotope composition, as saturation typically decreases with depth, favouring crystal growth over nucleation (Fike et al., 2015; Wilkin et al., 1996).

2.2 Stable sulfur isotope fractionation

Sulfur has four stable isotopes: ^{32}S (95.04%), ^{33}S (0.749%), ^{34}S (4.20%), and ^{36}S (0.0156%). These isotopes are regularly fractionated in processes involving sulfur species, especially biologically mediated reactions (Canfield et al., 2005). Biological processes tend to favour lighter isotopes over heavier ones which results in the reaction products' enrichment in lighter isotopes.

Isotopic compositions of ^{34}S relative to ^{32}S are typically used, as these are the most abundant. Isotopic compositions are presented in per mille (‰) relative to a standard according to the formula:

$$\delta^{34}S = \left(\frac{\left(\frac{^{34}S}{^{32}S}\right)_{Sample}}{\left(\frac{^{34}S}{^{32}S}\right)_{Standard}} - 1 \right) * 1000 \quad [‰] \qquad \text{(Eq. 1)}$$

The international standard for sulfur stable isotopes is the Vienna Canyon Diablo Triolite (VCDT), which represents the bulk $\delta^{34}S$ of the solar system ($\delta^{34}S$ = 0‰).

The fractionation factor α is used to describe the fractionation between two pools A and B.

$$\alpha_{A\text{-}B} = R_A/R_B \qquad \text{(Eq. 2)}$$

$$R = {}^{34}S/{}^{32}S \qquad \text{(Eq. 3)}$$

Fractionations are expressed using the following equation:

$$\varepsilon_{A-B} = (\alpha_{A-B} - 1) * 1000 \quad [‰] \qquad \text{(Eq. 4)}$$

For simplification, fractionations are also expressed as the change in isotopic composition between the two pools (A and B), which is approximately equal to the former (Canfield, 2001a):

$$\varepsilon_{A-B} = \delta^{34}S_A - \delta^{34}S_B \qquad \text{(Eq. 5)}$$

Different sulfur species are extracted from samples and measured to quantify fractionation between different sulfur pools. The fractionation values for specific processes like sulfate reduction and sulfide oxidation are generally measured through laboratory culture testing (Canfield, 2001a; Jørgensen et al., 2019a).

2.2.1 Microbial sulfate reduction

Regarding the sulfur cycle, the most extensive fractionation of sulfur stable isotopes is linked to microbial sulfate reduction. The well-mixed marine dissolved sulfate has a δ^{34}S value of 21‰ (Jørgensen et al., 2019a). Pure cultures have shown fractionations of 4–46‰ (average 18±10‰) (Canfield & Teske, 1996). Canfield (2001a) gathered previously reported results from natural culture tests that showed fractionations of 16–42‰. More recently, however, Sim et al. (2012) reported depletions up to 66‰ using cultures of sulfate-reducing microorganisms from coastal sediments in iron-deficient conditions. Jørgensen et al. (2019a) noted that the results obtained through culture tests do not best reflect the fractionation occurring in marine sediments because the in situ environmental conditions (e.g., organic matter availability) differ.

The extent of fractionation during microbial sulfate reduction depends on two main variables: sulfate concentration and the cell-specific sulfate reduction rate (Fike et al., 2015). Higher sulfate concentrations yield increased fractionations, whereas lower concentrations (and the resulting limited sulfate transport to the cell) generate low fractionations (Canfield, 2001b; Canfield et al., 2005; Habicht et al., 2002). Habicht et al. (2002) found that sulfate concentrations below 50–200 μM suppress isotope fractionation. A high cell-specific sulfate reduction rate (csSRR) results in lower fractionation, while a slower rate produces larger

fractionations (e.g., Leavitt et al., 2013; Sim et al., 2012). Therefore, in low sulfate concentrations large fractionation can still occur if cell specific SSR is low and vice versa (Jørgensen et al., 2019a). Moreover, Leavitt et al. (2013) demonstrated that electron donor (organic matter) availability, not sulfate concentration, controlled the extent of fractionation, with fractionation inversely correlating with organic matter concentration.

Sulfate reduction, favouring ^{32}S over ^{34}S, leads to Rayleigh-type distillation in a closed system (Fike et al., 2015). In closed or semi-closed systems, such as pore-waters with progressively decreasing seawater connection, as sulfate is reduced to sulfide, the remaining sulfate pool gets enriched in ^{34}S relative to ^{32}S. Consequently, the sulfide produced from this sulfate gets progressively more enriched in the heavier isotope as well (Fike et al., 2015). This is reflected in the depth profile of pore water $\delta^{34}S_{sulfate}$ and $\delta^{34}S_{sulfide}$ as both get progressively higher with depth until the sulfate methane transition zone (e.g., Masterson et al., 2022). In a closed system, all produced sulfide stays in the same sediment horizon and is gradually turned into sulfide minerals, thus the difference between porewater $\delta^{34}S_{sulfate}$ and $\delta^{34}S_{sulfide}$ at all depths is equal to ε in microbial sulfate reduction (Jørgensen, 1979). However, it is recognized that pore water is subject to diffusion in all sediments and the extent depends on factors like sedimentation rate, iron availability, and organic matter content (Fike et al., 2015; Halevy et al., 2023). According to a model constructed by Jørgensen (1979), under open system conditions, where sulfate and sulfide can freely diffuse, the isotopic difference between porewater $\delta^{34}S_{sulfate}$ and $\delta^{34}S_{sulfide}$ increases with depth, being lower than microbial fractionation at the sediment surface, but greater in deeper sediment horizons.

2.2.2 Sulfide oxidation and disproportionation

The oxidation of sulfide can further fractionate sulfur isotopes. Fractionation during biological sulfide oxidation to sulfur intermediates or sulfate is generally considered low (below 4‰) (Canfield, 2001a; Fike et al., 2015; Jørgensen et al., 2019a). However, significant fractionations (over 12‰) have been reported for specific sulfide-oxidizing bacteria (Pellerin et al., 2019).

Sulfur disproportionation can have substantial isotope effects (Canfield & Teske, 1996; Canfield & Thamdrup, 1994). While initial sulfate reduction fractionates sulfur by up to 47‰, repeated oxidation and reduction cycles can further fractionate sulfur, resulting in sulfides that

are highly depleted in ^{34}S relative to sulfate (Fike et al., 2015). Therefore, sulfur disproportionation is a mechanism that can produce isotopically light sulfides. The role of sulfur disproportionation in isotopic signals of sulfur species has been greatly debated, however, because sulfate reduction alone has produced large fractionations as well (Leavitt et al., 2013; Sim et al., 2011)

2.2.3 What signals are recorded in sedimentary pyrite?

Marine pyrites have shown depletions in ^{34}S by 24–71‰ with an average of 51±10‰ (Canfield & Teske, 1996). The precipitation of monosulfides and pyrite does not produce considerable fractionations (Böttcher et al., 1998), therefore, the isotopic composition of buried pyrite should reflect the isotopic composition of H_2S and S_8 from which it was formed (depending on the pathway) (Jørgensen, et al., 2019a). This implies that pyrite formed near the sediment surface is enriched in ^{32}S and the pyrite growing at depth gets gradually enriched in ^{34}S (Jørgensen et al., 2019a).

As a result, the isotopic signal of the bulk pyrite in the sample depends on two factors: microbial fractionation during sulfate reduction and isotopic distillation of sulfate and sulfide pools. The former is subject to sulfate concentrations and cell-specific sulfate reduction rates, while the latter depends on the openness of the sediment system (Fike et al., 2015). In the open system, where the diffusive exchange with the overlying water column with an original sulfate isotopic composition (around +21‰) is high, the isotopic difference between seawater sulfate and produced sulfide is equivalent to fractionation during microbial sulfate reduction (Claypool, 2004; Halevy et al., 2023). In a closed system, where sulfate is supplied through burial and diffusive effects are minimal, the apparent fractionation is smaller because the sulfate pool and produced sulfide get quickly enriched in ^{34}S, consequently yielding isotopically heavier pyrites (Halevy et al., 2023). In natural environments, the conditions are somewhere between those, whilst the openness of the system is related to sedimentation rates, sulfate concentrations, organic carbon availability, sediment porosity, and iron availability (Fike et al., 2015). Figure 3 shows the steady state dependence of $\delta^{34}S_{sulfate}$ and $\delta^{34}S_{pyrite}$ on the relative burial flux of pyrite.

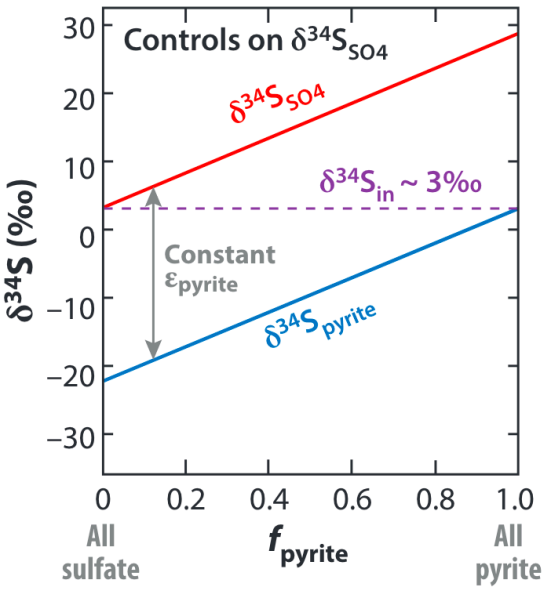

Figure 3. Schematic of the steady-state dependence of $\delta^{34}S_{sulfate}$ and $\delta^{34}S_{pyrite}$ on relative burial flux of pyrite (f_{pyrite}), assuming the seawater sulfate has an isotopic composition of $\delta^{34}S$ = 3‰ (from Fike et al., 2015).

In modern marine sediments, facial dependency is typically observed in the fractionations of sulfur isotopes (e.g., Pasquier et al., 2021; Wijsman et al., 2001). In shallow, organic-rich sediments, fractionations are typically smaller, but in typical deep-water sediments, where the availability of organic carbon is limited, fractionations are generally large. This can be explained by a change in system openness as diffusive effects increase in deeper waters (Claypool, 2004).

The isotopic signals from co-occurring sulfides (pyrite) and sulfates in sedimentary rocks have been widely used for interpreting ancient seawater chemistry and oxygenation (Fike et al., 2015). Over long timescales, sulfate burial relative to sulfide burial controls the ocean's oxygenation state and eventually the atmosphere's oxygen levels (Canfield, 2001a; Fike et al., 2015). Studies have suggested that other factors, including sedimentation rate and availability of reactive iron can influence these isotopic signals (J. Liu et al., 2020; X. Liu et al., 2019). The depositional environment has been proven to have significant effects on isotopic signals (Fike et al., 2015; Pasquier et al., 2021). Halevy et al. (2023) have recently proposed that it is primarily the distillation, not microbial sulfate reduction, that controls the isotopic differences of sulfur in pyrites, therefore shifting the focus from global ocean chemistry to local depositional environment when explaining sulfur isotopic signals.

In conclusion, the isotopic composition of different sulfur species in marine sediments is influenced by current processes (sulfate reduction, sulfide oxidation, disproportionation, etc.), past processes in the sediment that led to the formation of solid-phase sulfur, and interactions with isotopic signals in other sediment layers via the diffusion of sulfide and sulfate (Jørgensen et al., 2019a). Interpreting the isotopic signals is, therefore, complex and cannot be done without considering the depositional context (Pasquier et al., 2021).

2.3 The Baltic Sea

The Baltic Sea is a semi-enclosed brackish sea located in Northern Europe, with an area of 386,000 km² (Tuuling, 2011, p. 5). It represents a sensitive environment that suffers from various environmental challenges, including hypoxia and eutrophication. The average depth is 54 meters, but in the Landsort Deep north of Gotland, the deepest point of the Baltic Sea, the depth reaches 459 meters (Björck, 1995).

Through the Danish Straits, the Baltic Sea is connected to the North Sea, where the salinity is 35‰ (Tuuling, 2011, p. 7). The salinity of the surface water in the Baltic Sea gradually decreases as one moves away from the Danish Straits. In the Danish Straits, the salinity is about 8–10‰, and in the central part of the Baltic Sea, it is 6–8‰. In the farther parts of the Gulf of Bothnia and the Gulf of Finland, the water is essentially fresh. The low salinity of the Baltic Sea is mainly generated by three factors: the narrow connection to the ocean through the Danish Straits, the inflow of numerous rivers, and high precipitation combined with low evaporation due to the climate. The highest salinity in the Baltic Sea is found in deep water. Below the halocline, the salinity can reach 15–20‰ (Tuuling, 2011, p. 7). The thermocline is located at a depth of approximately 30 meters in the Baltic Sea (Björck, 1995).

The Baltic Sea suffers from extensive eutrophication due to excessive inflow of nitrogen and phosphorus. The deeper parts of the Baltic Sea are hypoxic or even anoxic (Hansson & Viktorsson, 2021). A hypoxic environment is one where the oxygen (O_2) content is below 2 mg/l (Conley et al., 2009). Historically, hypoxia has been a natural condition caused by the slow water exchange with the ocean due to topography, but climate change and eutrophication have increased its extent (Carstensen et al., 2014). Inflows of saline and oxygen-rich ocean water are rare and require specific water level, wind, and weather conditions (Hansson &

Viktorsson, 2021). The Baltic Sea is permanently stratified due to the density differences between saline and brackish water. These layers are separated by a sharp halocline, which is usually at a depth of 60–80 meters (Conley et al., 2009). The upper layer is constantly mixed with the atmosphere and is generally well-oxygenated. However, the bottom layer is not affected by the mixing of the surface layers. The decomposition of organic matter in deep water consumes the oxygen present in the water (Hansson & Viktorsson, 2021). When the amount of oxygen added through physical processes (water mass mixing) is lower than the amount consumed biologically, oxygen levels decrease, eventually creating hypoxic conditions (Conley et al., 2009). In extreme cases, anoxia (dissolved O_2 content of 0) can develop near the seabed. In the fall of 2021, 31% of the deep water in the Baltic Sea suffered from hypoxia and 20% from anoxia (Hansson & Viktorsson, 2021).

Despite political efforts in reducing nutrient inputs since the 1980s, eutrophication and low oxygen levels are still escalating. Over the past century, hypoxic areas have expanded tenfold (Carstensen et al., 2014). Hypoxic areas are expanding because large saline water inflow events are becoming rarer and increased eutrophication leads to greater organic material input (Hansson & Viktorsson, 2021). Climate warming is also expected to exacerbate this problem because higher temperatures decrease oxygen solubility, increase respiration rates, and magnify seawater stratification (Carstensen et al., 2014).

Due to the low salinity of the Baltic Sea, the sulfate reserve in the sediment pore water is relatively small. Extensive eutrophication and hypoxia result in enhanced organic matter accumulation in the sediments. Due to low oxygen content and high organic matter sedimentation rate, the biogeochemical zonation is concentrated near the sediment-water interface, and organic matter degradation is mostly dependent on sulfate reduction and methanogenesis rather than O_2 and metal oxides (Jørgensen et al., 2019a; Jørgensen & Kasten, 2006). This results in high sulfide production near the sediment surface and increases the risk of euxinia in the bottom waters (Jørgensen et al., 2019a).

3. Material and methods

3.1 Sulfur extraction line for acid volatile sulfide and chromium reducible sulfur

Chromium reducible sufur (CRS) distillation is a widely utilized technique developed by Canfield et al. (1986). This method uses hot acidic $CrCl_2$ which reacts with reduced sulfur species: acid volatile sulfide, pyrite, and elemental sulfur (S^0). The reduced sulfur is converted into H_2S gas, which is then precipitated as metal sulfide, commonly Ag_2S or ZnS.

Acid volatile sulfide (AVS) refers to the sulfide that is liberated as H_2S from the sediments when treated with HCl. In natural sediments, AVS is predominantly considered to represent iron monosulfides (FeS), but also Zn, Cu, and other metal monosulfides (Luther, 2005; Rickard & Morse, 2005). In practice, AVS and CRS are typically liberated sequentially by first treating the sample with HCl and then with $CrCl_2$. This allows AVS and pyrite sulfur (assuming minimal S^0 concentrations) to be collected separately.

The University of Tartu previously lacked the capability for chromium reducible sulfur distillation. As part of this study and the MESS (PSG944) project, an extraction line for AVS and CRS was constructed. The setup was inspired by the system established in D. A. Fike's laboratory at Washington University in St. Louis. Figure 4 shows the configuration of the extraction line at the University of Tartu.

The setup consists of a gas distribution system and an extraction system. The sample is placed into the reaction vessel prior to the reaction. A constant flow of N_2 gas is required to create and maintain anoxic conditions within the system. To initiate the reaction, the reactant (HCl for AVS or $CrCl_2$+HCl for CRS) is introduced through the side arm of the reaction flask. Once the reactant is added, the temperature is raised to the desired levels (65°C for AVS and 85°C for CRS). Nitrogen (N_2), serving as a carrier gas, brings the liberated H_2S through the water trap into the $AgNO_3$ trap, where it precipitates as Ag_2S. Ideally, the bubbling rate into the water trap should be about 1 bubble per second. Rapid bubbling may facilitate the loss of H2S from the extraction line, thereby inducing kinetic fractionation of S isotopes. The bubble sizes in the $AgNO_3$ trap should be as small as possible. The distillation takes about 1.5–2 hours for AVS and 2 hours for CRS, after which the precipitated Ag_2S is rinsed with distilled water and dried at low temperatures for further analysis.

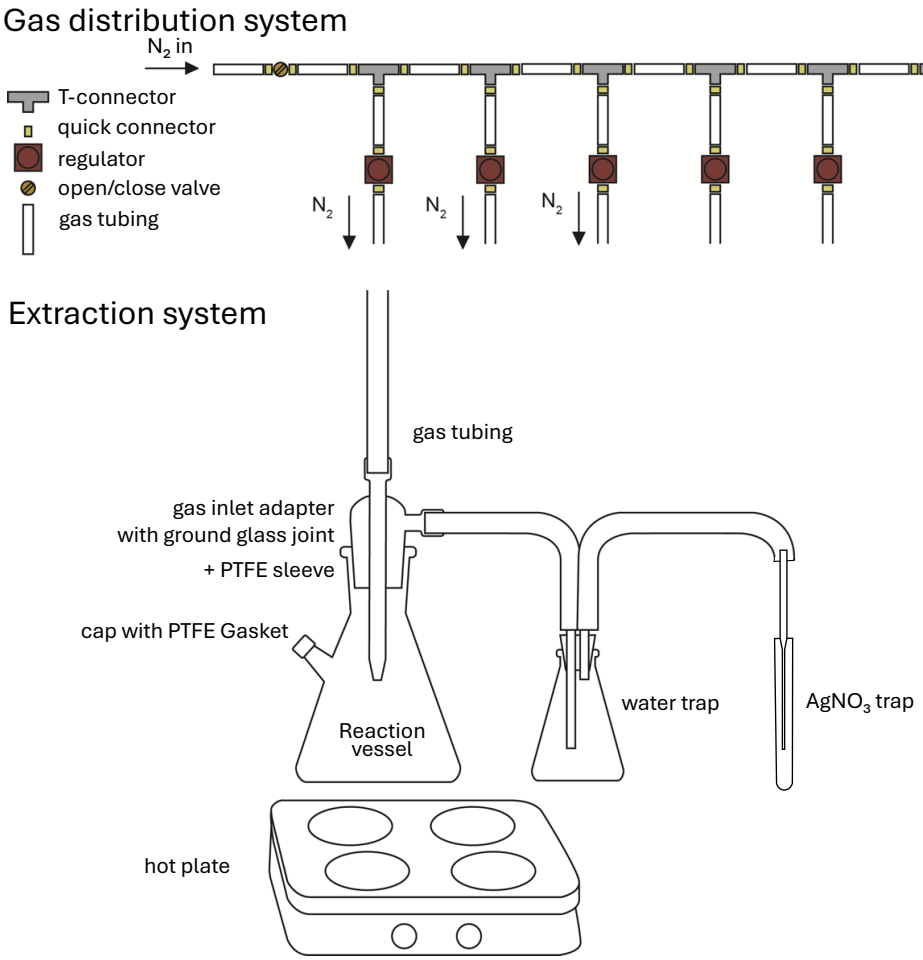

Figure 4. Schematic of the extraction system setup.

To test and validate the extraction system, tests were carried out with homogenized materials with known sulfide contents: a magnetite quartzite sample RK-000093 containing 11.9 wt% $Fe_{1-x}S$ (pyrrhotite) and a standard material EMS-1 Estonian Metalliferous Shale (Estonian alum shale) with a pyrite content of 4.8 wt% (standard deviation SD = 0.2, 1σ here and elsewhere) (Sardisco et al., 2022).

Acid volatile sulfide (AVS) was extracted from RK-000093 during two distillation cycles with 0.02 M $AgNO_3$ traps and 0.1 M $AgNO_3$ traps, and sample masses ranging from about 0.1 g to 0.5 g. A 25 mL solution of 6 M HCl was added to the samples to liberate the sulfide. The hot plate was set to 65°C except for two extraction lines, where hot plates without a thermostat were used (due to a malfunction of the regular equipment). In the extractions without a thermostat, temperatures possibly considerably exceeded 65°C.

Chromium reducible sulfur (CRS) was extracted from the EMS-1 Estonian Metalliferous Shale standard material. Given the relatively high organic matter content in this reference material, loss of ignition (LOI) analysis at 550°C was performed to estimate the organic matter concentration. This allowed the normalisation of the previously determined pyrite content (4.8 wt% by XRD) to the total sample mass, including the organic fraction. This approach provides a more accurate estimate of the true pyrite concentration in the bulk sample. The $CrCl_2$ solution was prepared a day prior to conducting the extractions. Two extraction cycles (a one-step and a two-step cycle) were performed with sample masses ranging from 0.1 to 1.0 g. For the one-step CRS extraction, a mixture of 25 mL $CrCl_2$ solution and 25 ml 6M HCl was used. In the two-step method, AVS was extracted with 25 mL 6M HCl followed by CRS extraction with a mixture of 25 mL $CrCl_2$ solution and 15 mL 6M HCl. Temperatures were set to 65°C for AVS and 85°C for CRS.

After extractions (within 1–2 days), the precipitated Ag_2S was rinsed 3–4 times with distilled water, dried at 70°C, and stored for isotope analysis. Isotope ratio mass spectrometry (IRMS) was used to determine the sulfur isotope composition of the extracted AVS and CRS fractions of both reference materials. Ideally, ~0.7–0.8 mg Ag_2S with ~0.3–0.4 mg V_2O_5 was weighed into tin capsules. If the obtained Ag_2S amounts were less than 0.7 mg, the entire sample was used, and the amount of V_2O_5 added was about 50% of the weighed sample. The isotope ratios were analysed with IRMS Delta V Plus + Flash HT+ Conflo IV at the University of Tartu IRMS laboratory. The instrument was calibrated against the IAEA international standards NBS 127 ($\delta^{34}S$ = 20.3 ‰) and IAEA-SO-6 ($\delta^{34}S$ = -34.1 ‰).

3.2 Study area

This study analyses three core samples from the Estonian territorial waters and the economic zone from the western Gulf of Finland to the northern Baltic proper. All samples were retrieved using a GEMAX-type corer during an expedition in June 2023 on board the Tallinn University of Technology's research vessel Salme. The sampling locations are shown in figure 5 and detailed in table 1. The water depths at the stations were 100 to 166 m and all locations can be characterised as mud accumulation areas. The retrieved cores are 43–55 cm in length.

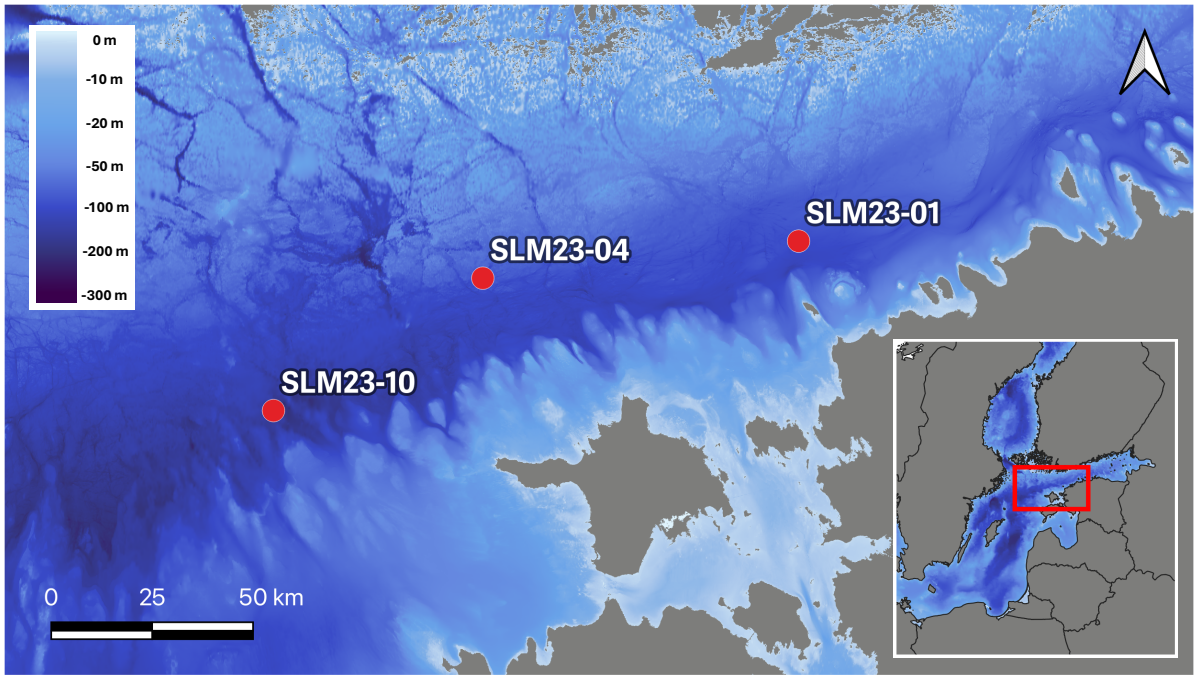

Figure 5. Map of the sampling locations (bathymetric map: EMODnet, 2024)

Table 1. Core location details.

Core name	Time	φ	λ	Water depth (m)	Core depth (cm)
SLM23-01	06.06.2023 14:11	59.4406	23.3370	100	55
SLM23-04	06.06.2023 21:17	59.344	21.9631	107	52
SLM23-10	07.06.2023 02:19	59.0322	21.0771	166	43

Sedimentation rates at stations SLM23-04 and SLM23-10 have been previously reported to be 0.103 ± 0.033 and 0.067 ± 0.033 cm·a^{-1}, respectively (Liira et al., 2024). The sedimentation rate in SLM23-01 is expected to be higher due to its proximity to the coastline.

All coring locations are situated below the wave base as well as below the permanent halocline and the thermocline. The temperature of the bottom water is around 6.5–7°C, and the salinity is around 11 g/kg (Estonian Marine Institute, 2023). According to the same dataset, the water around the study areas is hypoxic below ~80 m depths. There is no measured data about the redox states of the bottom waters close to the sediment surface. As an indirect method, the uranium and molybdenum enrichment factors of the sediments indicate (ir)regularly euxinic (anoxic and sulfidic) conditions in station SLM23-01 and permanently euxinic conditions in station SLM23-10 (Lahtvee, 2023).

At station SLM23-01, porewater sulfate concentrations have earlier been determined from a core sampled in September 2022. This study found that sulfate is depleted within the first 10 cm depth with a rate of 0.726–1.068 mol/m2yr (calculated using a diffusion model) (Roopõld, 2023). This is a relatively high rate compared to the results of other studies in the Baltic Sea (e.g., Jørgensen et al., 2019b; Piker et al., 1998).

The sulfur isotope composition of seawater sulfate has not been measured for the specific study locations. However, a study done by Ikonen et al. (2022) reported $\delta^{34}S$ values of seawater sulfate around 21–22‰ in the coastal bottom waters of the Gulf of Finland. Moreover, the $\delta^{34}S$ values of seawater sulfate are considered to be very stable, around +21‰, in today's oceans (Jørgensen, 2021).

3.3 Analyses with Baltic Sea sediments

Right after retrieval, cores SLM23-04 and SLM23-10 were sliced into subsamples with 1 cm intervals and frozen. Core SLM23-01 was frozen as a whole and later cut into subsamples with 2 cm intervals. Then, 10 to 11 subsamples were chosen from each core for further analysis. About 10 to 30 g of frozen sample was freeze-dried (at the Institute of Chemistry, University of Tartu) to prevent oxidation. The freeze-dried samples were stored below -5°C.

For mineralogical analysis, the samples were powdered using a mortar and pestle and placed in sample holders. Each sample was analysed with a Bruker D8 Advance XRD instrument (University of Tartu XRD lab). The diffractograms were interpreted using the Rietveld refinement-based software Topaz.

To estimate elemental abundances in the samples, energy dispersive X-ray fluorescence (ED-XRF) analysis was done using the Brucer TRACER 5i instrument with Oxide3phase method and 180 second masurement time. The samples were prepared by powdering and pressing them into a pellet with a hydraulic press. This study recognizes the lack of matrix-matched calibration and the subsequent unreliability of the results. This ED-XRF analysis was conducted to estimate the depth profiles of Fe and S in the cores. Additionally, inductively coupled plasma mass spectrometry (ICP-MS) analysis has been previously conducted for

samples of cores SLM23-04 and SLM23-10 and reported in the Geological Survey of Estonia project report (Liira et al., 2024).

Using the newly developed sulfur extraction line for the chromium-reduction method at the University of Tartu, AVS (S^{2-}) and CRS (S^{1-} ≈ pyrite sulfur) were extracted from 6 samples from each core. Based on the pyrite content determined by the XRD analysis, 0.5–1.3 g of freeze-dried samples was used. First, acid volatile sulfide (monosulfide) was collected by the reaction with 25 mL 6 M HCl on a 65°C hot plate for ~1.5h (AVS technique). Then, for CRS extraction, $CrCl_2$ + 6 M HCl mixture (25 + 15 ml) was added to the sample and heated to 85°C. The liberated H_2S was precipitated as Ag_2S in a 0.1 M $AgNO_3$ trap. Ag_2S was rinsed three times with distilled water and dried at 60°C before weighing and IRMS analysis.

Isotope ratio mass spectrometry (IRMS) was used to determine the sulfur isotope composition of the CRS fraction. ~0.7–0.8 mg Ag_2S with ~0.3–0.4 mg V_2O_4 was weighed into tin capsules and analysed with IRMS Delta V Plus + Flash HT+ Conflo IV at the University of Tartu IRMS laboratory. The instrument was calibrated against the IAEA international standards NBS 127 ($\delta^{34}S$ = 20.3 ‰) and IAEA-SO-6 ($\delta^{34}S$ = -34.1 ‰).

From a few samples with higher pyrite concentrations (SLM23-01-48, SLM23-04-16, SLM23-10-0 and SLM23-10-16), images of pyrite framboids were taken using a scanning electron microscope (SEM) ZEISS EVO 15MA in variable pressure mode. Before SEM analysis, sample preparation included the separation of the <63 μm grain fraction from wet samples through wet-sieving. Subsequently, the samples were dried at 70°C. The obtained <63 μm fraction was prepared on SEM carbon adhesive tabs.

For estimating organic matter concentrations in the samples, loss-on-ignition analysis at 550°C (LOI 550) was conducted. For the samples of cores SLM23-04 and SLM23-10, the LOI 550 results have been obtained from the Estonian Geological Services project report (Liira et al., 2024). For SLM23-01, the analysis was conducted as part of this study. All wet samples were first dried at 105°C for >15 hours. Then, about 2–5 g of dried sample was combusted at 550°C for 3 hours.

4. Results

4.1 Sulfur extraction line validation

Acid volatile sulfide (AVS) extractions using the magnetite quartzite sample RK-000093, containing 11.9 wt% of $Fe_{1-x}S$ (pyrrhotite), yielded poor AVS recoveries (table 2, figure 6). On average, only 6.8% (standard deviation SD = 7.1) of expected AVS was captured in the extractions. It is important to note that with 11.9 wt% $Fe_{1-x}S$ (pyrrhotite) concentrations, the expected AVS amounts for all samples would have exceeded the trap capacities, but trap capacity was reached only once.

Table 2. AVS test conditions and results for RK-000093 reference material

Sub-sample	Trap molality (M)	Sample mass (g)	Expected Ag_2S (g)*	Obtained Ag_2S (g)	Reaction time (h)	Notes
RK93-1	0.02	0.1007	0.0338	0.0002	01:55	
RK93-2	0.02	0.2201	0.0738	0.0007	01:55	
RK93-3	0.02	0.3076	0.1032	0.0156	01:55	
RK93-4	0.02	0.5359	0.1798	0.0047	01:55	
RK93-5	0.1	0.2473	0.0830	0.0182	01:50	Temperature not fixed
RK93-8	0.1	0.2471	0.0829	0.0091	01:50	Temperature not fixed
RK93-9	0.1	0.2547	0.0854	0.0035	01:50	
RK93-10	0.1	0.2458	0.0825	0.0052	01:50	
RK93-11	0.02	0.2458	0.0825	0.0012	01:50	
RK93-12	0.02	0.2462	0.0826	0.0034	01:50	

*assuming 11.9 wt% pyrrhotite concentration in sample

During the AVS extractions utilizing 0.02 M $AgNO_3$ traps, the trap solution turned from clear to transparent green to dark brown during the extraction, accompanied by significant Ag_2S precipitation on the test tube walls. The presence of a strong smell of H_2S indicated substantial leaks in the system. Moreover, the gas flow was exceptionally sensitive and the bubbling rates varied considerably between extraction lines. On average, only 4.1% of expected AVS precipitated.

Using 0.1 M $AgNO_3$ traps, the trap solutions turned slightly yellow in the beginning, but cleared up by the end of the extraction cycle. Precipitates flowed loosely in the test tube and sank to the bottom, with minimal precipitation happening on the test tube walls. On average, 10.8% of expected AVS precipitated. Notably, the extractions conducted at temperatures likely exceeding the fixed 65°C, due to the absence of a thermostat, yielded better results.

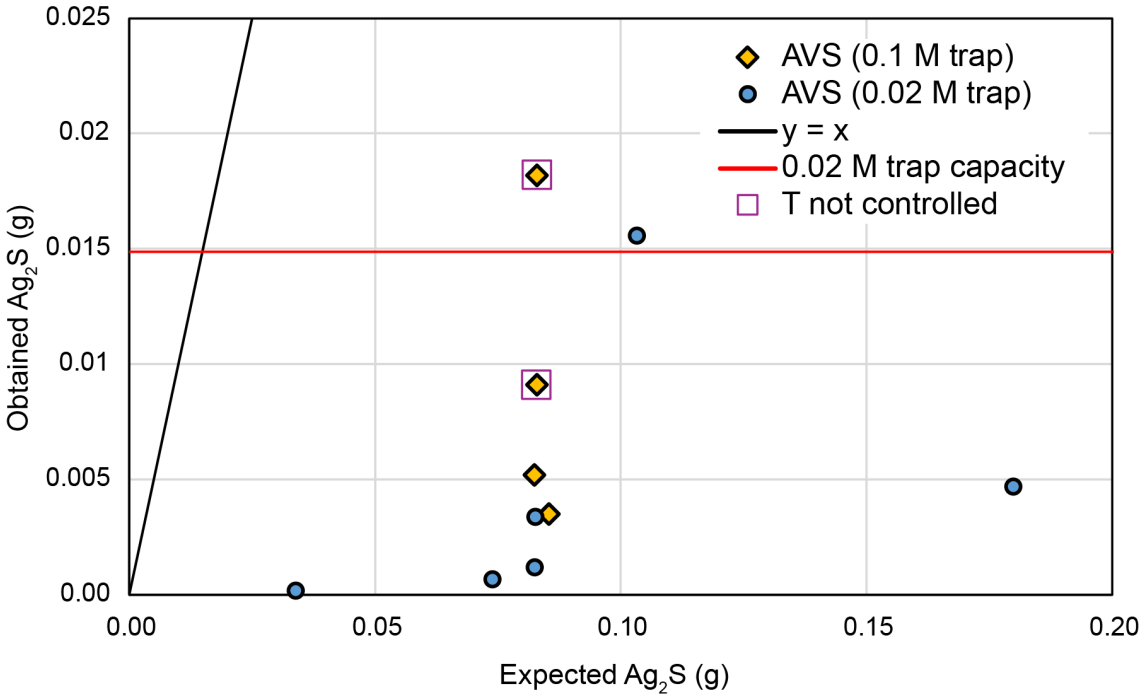

Figure 6. Expected and obtained Ag_2S precipitation during AVS extraction from RK-000093 with two 0.02 M $AgNO_3$ trap (blue dots) and 0.1 M $AgNO_3$ trap (yellow diamonds).

Recoveries from CRS tests using the EMS-1 standard material are illustrated in figure 7. Test conditions are in table 3. Loss of ignition analysis at 550°C estimated the organic matter concentration at 10.8 wt%. This means that a more accurate pyrite concentration of EMS-1 is 4.3 wt%.

In the two-step extractions, AVS recovery from EMS-1 was noticeable but minimal. Consequently, the obtained CRS amounts are very similar in both one-step and two-step extractions. Expectedly, Ag_2S precipitation reached the limit (0.074 g Ag_2S) set by the trap molality when sample masses exceeded 0.375 g. Excluding these tests, the obtained Ag_2S amounts coincide relatively well with the expected values and the average CRS recovery was 77%.

In all CRS extractions, Ag_2S precipitation began right after adding the $CrCl_2$+HCl solution, before raising the temperature. Most extraction lines experienced unstable gas flows and needed to be adjusted every ~1-10 minutes. Occasionally, these lines experienced more vigorous bubbling into the trap.

Table 3. Test conditions for AVS and CRS extractions and results for EMS-1 standard material.

Sub-sample	Extraction type	Sample mass (g)	Expected Ag_2S (g)	Obtained Ag_2S (g)		Extraction time (h)		Notes
			CRS	AVS	CRS	AVS	(CRS)	
EMS1	CRS	0.1012	0.0180	-	0.0138	-	02:00	
EMS2	CRS	0.2523	0.0448	-	0.0303	-	02:00	Especially unstable gas flow
EMS3	CRS	0.5006	0.0889	-	0.0718	-	02:00	
EMS4	CRS	1.0590	0.1881	-	0.0726	-	02:00	
EMS5	AVS+CRS	1.0270	0.1824	**	0.0717	01:25	02:00	
EMS6	AVS+CRS	0.5053	0.0897	1E-04	0.0726	01:25	02:00	
EMS7	AVS+CRS	0.2448	0.0435	1E-04	0.0422	01:25	02:00	
EMS8	AVS+CRS	0.1004	0.0178	***	0.0119	01:25	02:00	AVS precipitation only on the pipette tip, trap not changed for CRS

*assuming 4.3 wt% pyrite concentration in the sample
**some precipitation, but all lost during rinsing
***not obtainable amount

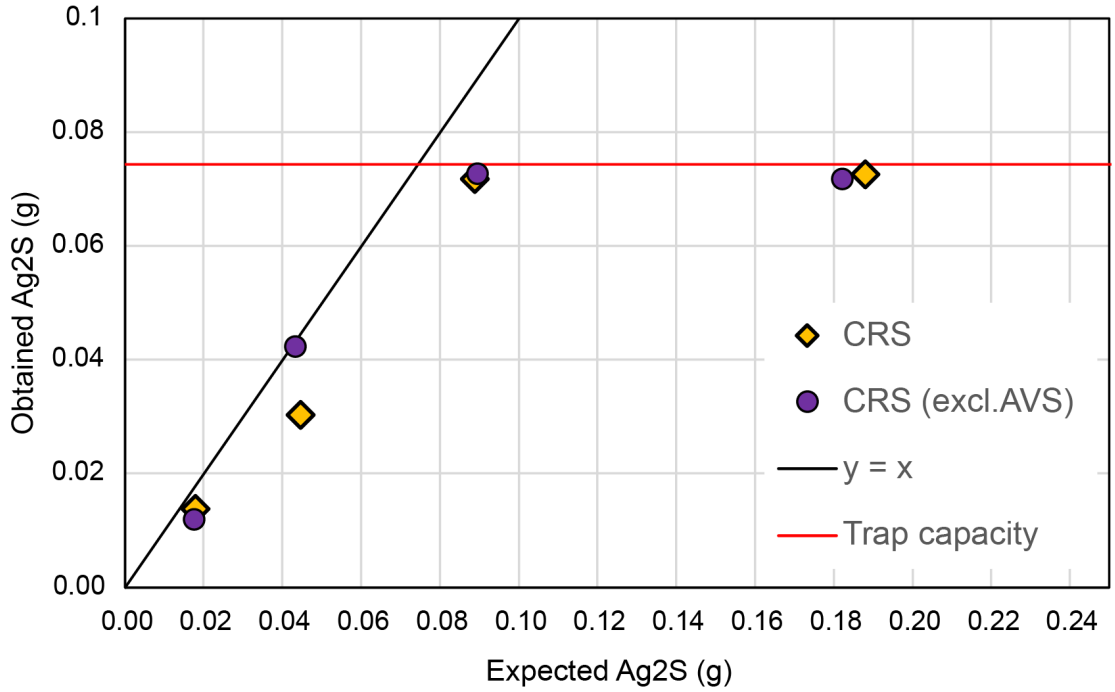

Figure 7. Expected and obtained Ag_2S precipitation during AVS extraction from EMS-1 standard material using 0.1 M $AgNO_3$ trap solutions.

The isotopic compositions of AVS in RK-000093 and AVS and CRS in EMS-1 are displayed in table 4 and summarized as boxplots in figure 8. The isotopic compositions of the AVS in RK-000093 varied from -2.89‰ to 0.47‰. The CRS fraction of EMS-1 showed $\delta^{34}S$ values from -18.65‰ to -17.40‰. In the two-step extraction method, AVS was removed beforehand,

exhibiting an isotopic composition of -16.35‰. The isotopic composition of the CRS fraction excluding AVS varied between -19.05‰ and -17.48‰.

Table 4. Isotopic compositions of all subsamples of RK-000093 and EMS-1 with average, median and standard deviation values.

RK-000093		EMS-1					
AVS		CRS		CRS (excl. AVS)		AVS	
Sub-sample	$\delta^{34}S_{VDCT}$ (‰)	Sub-sample	$\delta^{34}S_{VDCT}$ (‰)	Sub-sample	$\delta^{34}S_{VDCT}$ (‰)	Sub-sample	$\delta^{34}S_{VDCT}$ (‰)
RK93-3	-1.15	EMS1	-17.40	EMS5	-19.05	EMS6+ EMS7	-16.35
RK93-4	-0.88	EMS2	-17.97	EMS6	-18.73		
RK93-5	-1.40	EMS3	-17.84	EMS7	-17.48		
RK93-8	0.47	EMS4	-18.65	EMS8	-18.69		
RK93-9	-0.93						
RK93-10	-0.98						
RK93-11	-2.89						
RK93-12	-2.24						
Average	-1.25	Average	-17.97	Average	-18.49		
Median	-1.06	Median	-17.91	Median	-18.71		
SD	1.00	SD	0.51	SD	0.69		

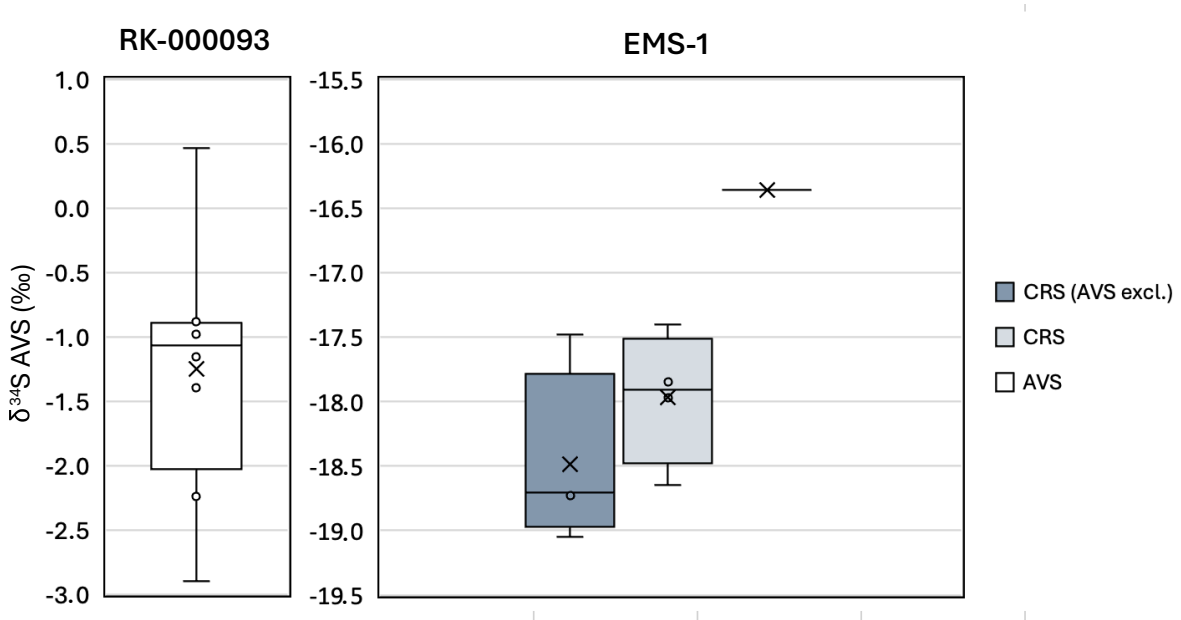

Figure 8. Box plots of the sulfur isotopic compositions of AVS from RK-000093 (left) and AVS and CRS from EMS-1 (right). The $\delta^{34}S$ is relative to Vienna Canyon Diablo Triolite (VCDT) standard.

4.2 Sediment characteristics

The sediment in all stations can be characterized as silty black mud (figure 9). The smell of H_2S was noticed with all fresh cores. With depth, the colour of the sediments changed gradually from black to dark grey.

Water content (figure 9; supplementary table 1) decreases with depth, showing increasing compaction towards deeper layers. It should be noted that water content estimations are possibly defective because frozen samples have not been homogenised before drying. This could especially be a problem with the upper interval of the SLM23-01 core, which was frozen prior to slicing. Moreover, during freezing, the ice had segregated from the majority of the sediment. Therefore, the water content strongly depended on the region the subsample was taken within the frozen slice of the core.

Loss of ignition at 550°C is an indication of the amount of organic matter in the dry sediment (figure 9; supplementary table 1). In the upper 1-2 cm, the highest organic matter content, 23.4wt%, is found in the westernmost station (SLM23-10) and lowest (11.3 wt%) in the easternmost (SLM23-01). While in SLM23-01, the concentration gradually decreases with depth from ~11 wt% to ~7 wt%, the other two cross-sections show a sharp decrease in the upper 10 cm and a stabilization at around 6–7 wt% below 10–20 cm sediment depth.

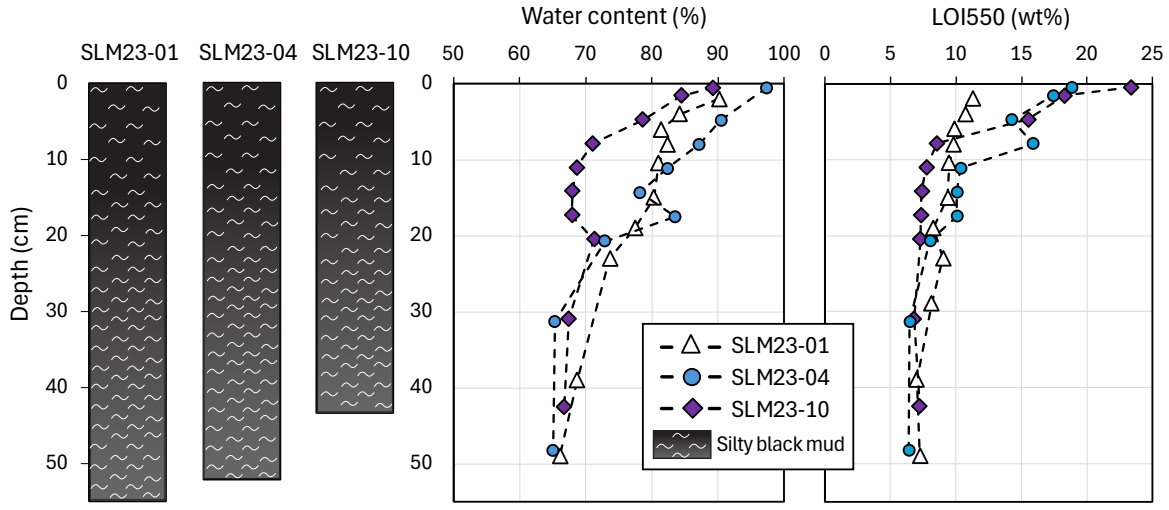

Figure 9. Sediment profiles and water content, and LOI 550 (organic matter) results. The data for SLM23-04 and SLM23-10 originates from Liira et al. (2024).

4.3 Sediment mineralogy and chemistry

The mineralogical composition of the sediments is shown in figure 10 and supplementary table 2. Because XRD only analyses the crystalline phase, the results have been normalised to account for organic matter concentrations (LOI 550) in the sediment. High halite (NaCl) concentrations at the top layers of the sediment are an indication of high water content. As a result, the seemingly low concentrations of other mineral phases in the upper 5–10 cm of sediment do not reflect the actual mineralogy of the sediment solid phase.

In SLM23-01, pyrite concentrations gradually increase with depth from about 2 to 5 wt% while other mineral phases stay comparatively stable. In the other two stations, pyrite abundance fluctuates within the profile. There is a clear front in SLM23-04 at 18 cm depth where pyrite concentrations reach 7 wt%. This is accompanied by higher quartz abundance and lower clay mineral (illite), K-feldspar, and plagioclase concentrations. However, the pyrite fluctuations in SLM23-10 do not seem to correlate with other mineral phases.

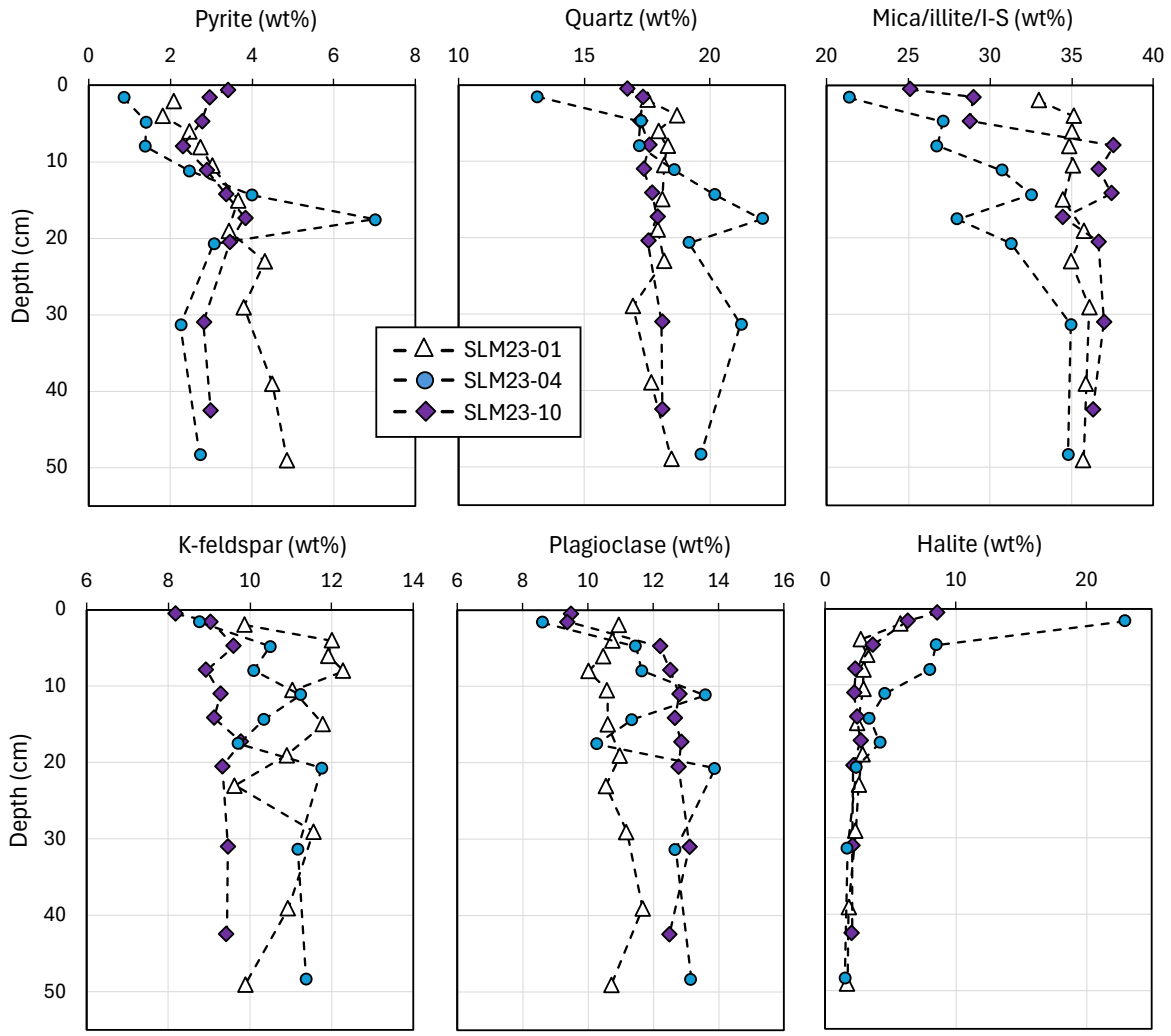

Figure 10. Pyrite, quartz, mica/illite, K-feldspar, plagioclase, and halite concentrations analysed with XRD. All concentrations have been normalised to account for organic matter in the samples.

The elemental abundances of Fe and S in the sediment are shown in figure 11 and supplementary table 3. The ICP-MS results and ED-XRF results correlate relatively well with R^2 values of 0.9996 for Fe and 0.9885 for S, while considering that ICP-MS results are more reliable, ED-XRF slightly underestimates the concentrations (see supplementary figure 1).

Iron concentrations in the sediments are lower at the sediment surface but quickly increase to around 4–5 wt% with depth, where they stay relatively stable. Sulfur concentrations fluctuate between 0.5 wt% and 3 wt%, but slightly decrease from ~1.5 to ~0.8 wt% with depth in SLM23-04 SLM23-10.

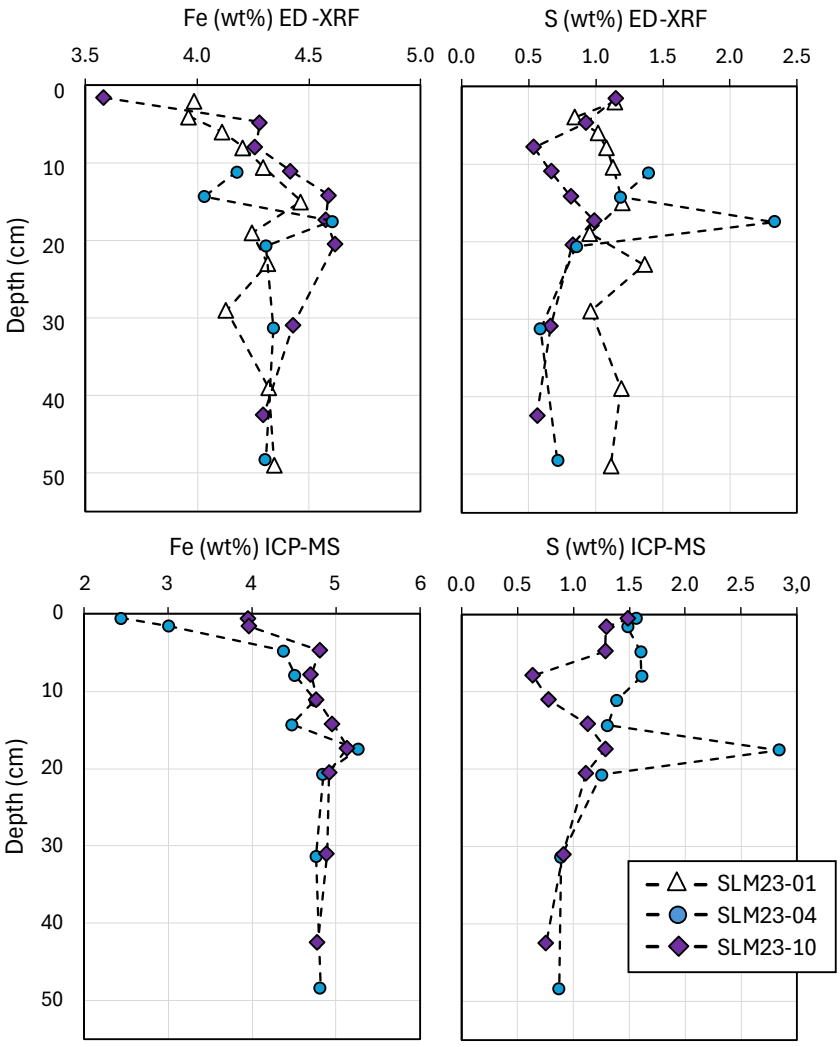

Figure 11. Fe and S concentrations measured with ED-XRF and ICP-MS. ICP-MS results are from Liira et al. (2024).

Framboidal pyrites were found in all sediment samples analysed with SEM (figures 12 and 13). Most pyrite framboids were in clusters and various micro-settings associated with organic substrates. These include algal cell remains (figures 12A and 12B), foraminifera (figure 13C), and organic films (for example, figures 13A, 13D, and 13F). In most framboids, octahedral or cubic microcrystals are not attached to one another but appear to be held together by a thin surrounding film. In many cases, the framboids show signs of disruption, with individual microcrystals having detached or broken loose (figures 12C and 12D, figures 13B and 13C). In certain framboid clusters in SLM23-10, microcrystals appear fused together, suggesting that crystal growth persisted during diagenesis (figure 13C). The sizes of the observed framboids

ranged from a few μm to 100 μm. In addition to pyrite, one larger barite ($BaSO_4$) particle was observed (figure 13C).

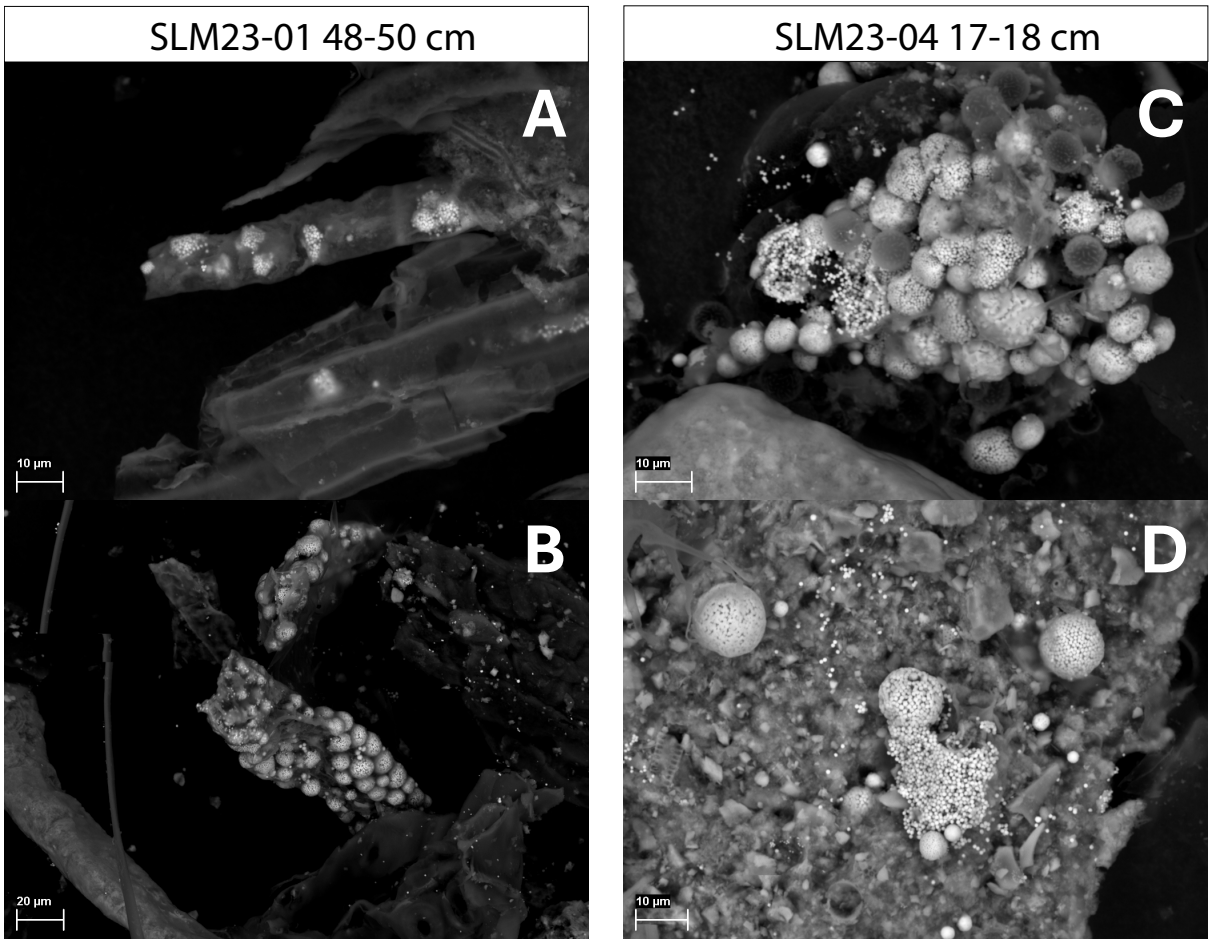

Figure 12. SEM secondary electron images of pyrites from station SLM23-01 from depth range 48–50 cm (A and B) and from station SLM23-04 at 16–17cm (C and D)

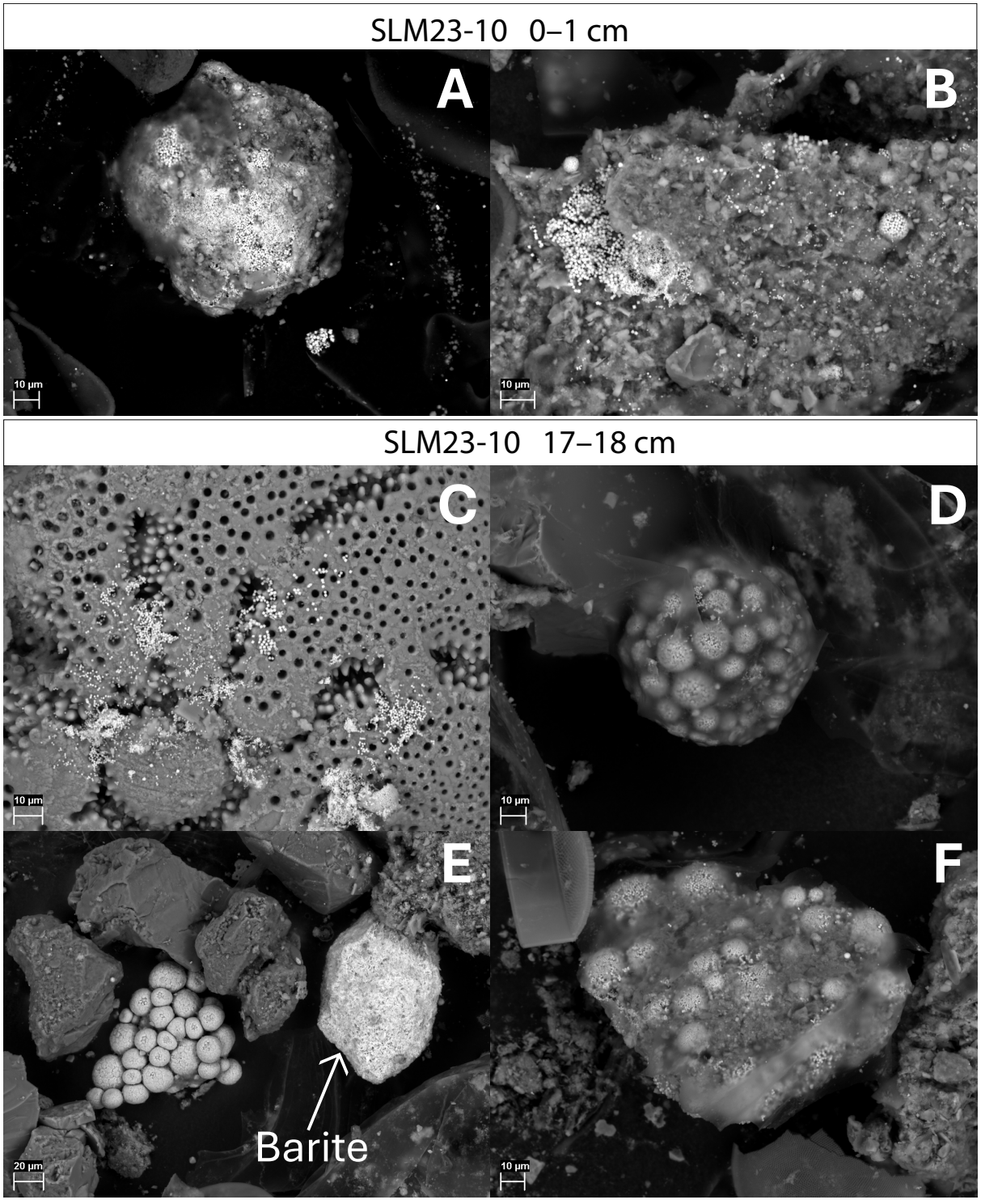

Figure 13. SEM secondary electron images of pyrites from station SLM23-10 from depth range 0–1cm (A and B) and 17–18cm (C–F).

4.4 Acid volatile sulfide, chromium reducible sulfur, and sulfur isotopes

Small amounts of AVS were detected during the extractions in all sediment samples. Weighing these amounts would have required a more sensitive scale than was available, but gross estimation shows that the concentrations of AVS (S) were below 0.01 wt% in all the samples except for two samples at station SLM23-04. At depths 4–5 cm and at 11–12 cm, AVS (S) concentrations were about 0.011 wt% and 0.03 wt%, respectively.

The extracted CRS amounts are shown in figure 14. These, however, are on average only 0.35 times the expected CRS sulfur in the sediments calculated from pyrite concentrations (see supplementary figure 2).

The isotopic compositions of AVS and CRS are shown in figure 14 and supplementary table 4. Except for some outliers, CRS gets gradually more enriched in ^{34}S with depth. The AVS, however, does not show such enrichments with depth, but stays relatively similar across the profile. In SLM23-04, the $\delta^{34}S_{CRS}$ profile shows a negative deviation (by about 10‰) from the gradual ^{34}S enrichment toward lighter isotopes at around 18 cm depth.

In the topmost ~11 cm of sediments, the isotopic compositions of CRS are notably distinct and become more depleted in ^{34}S westward. The $\delta^{34}S_{CRS}$ values of the topmost sample going westward are -9.7‰ (SLM23-01), -19.4‰ (SLM23-04), and -32.4‰ (SLM23-10). The $\delta^{34}S_{AVS}$ values show the same westward pattern, but in SLM23-04 and SLM23-10, the AVS is more enriched in ^{34}S than CRS in the upper sediments. In SLM23-01, the isotopic compositions of AVS and CRS are in the same range ($\delta^{34}S_{CRS}$ between -9.7 and -2.4, $\delta^{34}S_{AVS}$ between -11.5 and -2.2) within the upper 30 cm of the sediment.

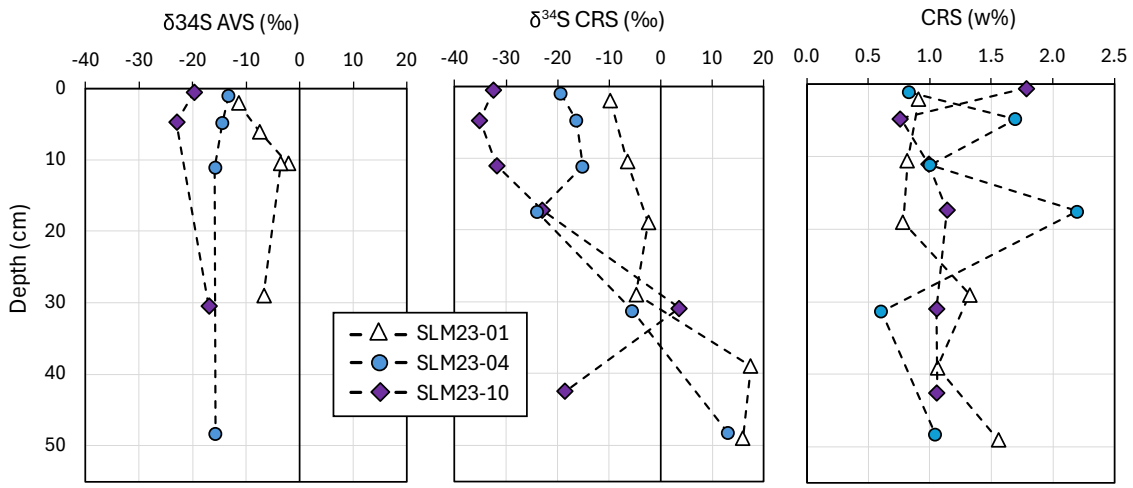

Figure 14. The $\delta^{34}S$ profiles of AVS and CRS and CRS concentrations. The $\delta^{34}S$ is relative to Vienna Canyon Diablo Triolite (VCDT) standard.

5. Discussion

5.1 Sulfur extraction line validation

The results of the experimental extraction line tests indicate that the overall recovery of AVS is low (on average 10.8% with 0.1 M $AgNO_3$ traps) within this extraction system. The CRS exhibits significantly higher recoveries (average 77%). It is important to acknowledge that the pyrrhotite concentrations in the sample RK-000093 and the pyrite concentrations in the sample EMS-1 have been determined using X-ray diffraction (XRD) with relatively few measurement replications. This may yield semi-quantitative results, potentially leading to inaccuracies in the AVS and CRS recovery estimations presented in this study.

The 0.02 M $AgNO_3$ traps yielded lower recoveries than 0.1M traps in AVS tests. This suggests that the 0.02M trap is not concentrated enough to effectively precipitate the H_2S bubbling into the trap.

One potential source for the losses in AVS and CRS is the leakage of H_2S from the system. Most joints in the setup were covered with parafilm. Therefore, the most probable source for the leakage is the $AgNO_3$ trap. Too large bubbles and/or too vigorous bubbling rates could result in large losses. The gas flow in the extraction line is rather sensitive, and reaching the right bubbling rate (1–3 bubbles per second) is difficult. In some cases, the gas flow was exceptionally sensitive and the bubbling rates varied considerably between extraction lines. This possibly contributed to the large leaks and variabilities in precipitated Ag_2S amounts. Moreover, precipitating Ag_2S can clog the pipette and change the gas pressure needed to bubble into the trap. This means that the gas flow needs to be adjusted every 1–10 minutes during the first half of the extraction cycle, which is suboptimal for effective operation of the extraction line.

The discrepancy between AVS recoveries and CRS recoveries makes us believe that, apart from leakage, other factors might have played into the notably low yields in the AVS tests. These include the reactant concentrations, reaction temperature, and/or human errors. To confirm that, these tests should be repeated with variations in reaction conditions. Until then, the AVS extraction cannot be used for quantitative estimations.

The variability of the isotopic values of sulfur fractions in one material is notable, up to ~3.5‰. Considering the materials are well homogenised, the cause of this effect lies within the extraction or analysis method. The largest variability was observed within the AVS tests with RK-000093, which experienced noticeably more leaks than tests with EMS-1. The CRS in EMS-1 showed isotopic variability of up to ~1.5‰. This means that the reason for the $\delta^{34}S$ variability was most probably the kinetic fractionation through the loss of H_2S during bubbling. Therefore, the extraction method fractionates considerably less if no leaks are present in the system, recognisable by the absence of a H_2S odour.

In conclusion, further tests with certified reference materials should be conducted along with modifications to the extraction methodology and setup, especially to the gas distribution system. Regardless, the variability of $\delta^{34}S$ in natural sediments and sedimentary rocks is usually large enough to draw reliable conclusions even with variations within 3–4‰.

5.2 Insight into the sulfur cycle and its contributing factors in the Baltic Sea

Organic matter:

The incorporation of organic matter in the sediments is heavily influenced by the primary productivity in the surface waters and the oxygen concentrations at the sediment-water interface (e.g., Rullkötter, 2006). In the Baltic Sea, which suffers from eutrophication and a large extent of hypoxic and anoxic bottom waters, both aspects favour the accumulation and preservation of organic matter.

The fact that organic matter concentrations (LOI 550) close to the sediment surface were largest (23.4 wt%) in the westernmost station SLM23-10 and decreased towards the mouth of the Gulf of Finland (18.7 wt% in SLM23-04 and 11.3 wt% in SLM23-01), may indicate that the availability of free oxygen in the water column decreases westward. The proximity to land could also play a role, as the sedimentation rates of inorganic sediments are possibly higher closer to land, decreasing the overall bulk organic matter concentration in the sediments.

The vertical distribution of organic matter concentrations in the sediment reflects the degradation of organic matter (Rullkötter, 2006). The deeper the sediment is buried, the more time it has had to degrade, therefore, the organic matter concentration decreases with depth.

This decrease can be seen in all the stations until a stabilization at around 6–7 wt% below 10–20 cm, possibly when more labile organic matter has been consumed. However, one must consider that part of this effect is caused by an increase in organic matter sedimentation rates in recent times (Carstensen et al., 2014).

Sediment chemistry and mineralogy:

As organic matter is degraded by sulfate reduction in the sediments, the sulfate in the pore water is turned into H_2S, of which a part is incorporated into sulfide minerals, predominantly iron sulfides (e.g., FeS and pyrite). In the studied stations, pyrite forms already at the sediment-water interface. A gradual increase of pyrite concentration with depth is expected. However, only station SLM23-01 exhibits such a profile (figure 10). In the other two stations, pyrite fluctuates within the profile. This is also seen in the correlation plots between organic matter concentrations and pyrite in the sediments (figure 15), where only SLM23-01 shows a clear correlation. There is a weak correlation between pyrite and organic matter concentrations in SLM23-04 (outlier removed) and no relation between these variables in SLM23-10, which indicates that other factors besides organic matter degradation and sulfate reduction play a role in pyrite abundances.

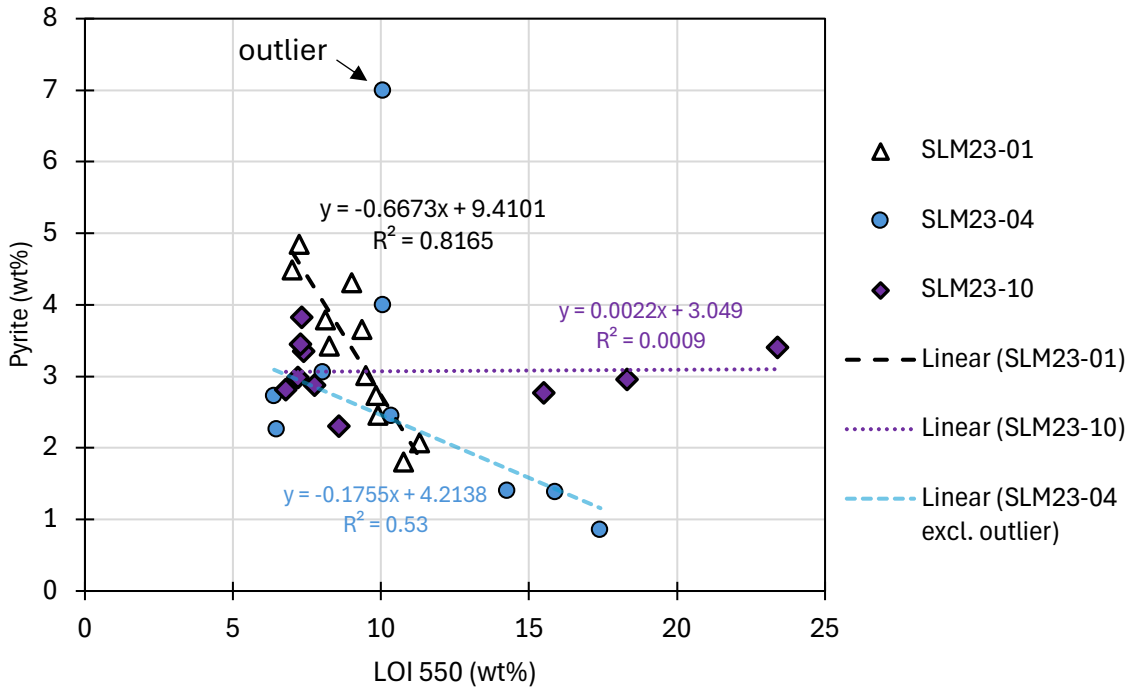

Figure 15. Pyrite concentrations plotted against LOI 550 (organic matter). The outlier (SLM23-04 18 cm) has been removed from the trendline estimation.

The large peak in pyrite concentrations accompanied by a peak in quartz concentrations at ~17-18 cm at station SLM23-04 (see figure 10) might indicate a single event or a period of increased terrigenous material influx, which created favourable conditions for pyrite formation (e.g., increased iron availability). Although the extracted AVS amounts were low, the concentrations seemed to be considerably greater at around 11–12 cm depth in core SLM23-04. This indicates a shift between the AVS and pyrite peaks. I hypothesise that this is because FeS forms intensively at a depth of 11–12 cm through the reaction between H_2S and reactive iron and is subject to diffusion into lower sediment layers, where it is transformed into pyrite under favourable conditions.

The abundances of S and Fe in the samples match with the mineralogical observations. The differences are brought about by the fact that, besides pyrite, Fe and S are present in other phases as well. Iron in the samples includes Fe in pyrite, Fe in other mineral phases (e.g., Fe-oxides), and Fe in porewater, while sulfur includes sulfur in sulfide minerals and sulfate of which pyrite sulfur and porewater sulfate contribute the most.

CRS amounts recovered during the extractions do not coincide well with the pyrite concentrations (supplementary figure 2). Therefore, pyrite concentrations from XRD analysis are used for further data interpretation.

Pyrite framboids

The occurrence of pyrite framboids in the sediments confirmed that pyrite in the sediments is authigenic. Additionally, SEM images (figures 12 and 13) revealed that most of the framboids are associated with biogenic substances. These substances, in which most of the pyrite was observed, can serve as diffusion-limiting spaces where supersaturation for crystal nucleation and growth can occur. The organic substance itself might be the source of electrons that fuel microbial sulfate reduction.

Due to the removal of <63 μm particles by wet sieving, the smaller pyrite crystals and framboids might have been lost before imaging. However, pyrite framboids as small as a few μm attached to larger sediment grains were observed. The larger framboids were up to 100 μm in size. Typically, the sizes of framboids formed in euxinic water column are <10 μm, while framboids formed in the sediments can develop larger sizes (Wilkin et al., 1996). Therefore,

the larger >10 μm framboids observed have most probably been formed within the sediment, while the origin of smaller-sized framboids cannot be distinguished.

The size and texture distribution of pyrite within the depth profile could be studied further, as it can provide insight into pyrite formation in natural sediments and its influence on isotopic signals.

CRS isotope composition

Analysing the isotope compositions for AVS and CRS, one must keep in mind the method variability (up to ~3.5 ‰) seen in tests with reference materials (see section 4.1 Sulfur extraction line validation). The $\delta^{34}S_{CRS}$ values in the studied samples ranged from -35.1‰ to 17.4‰, which is far greater than the analytical uncertainty of the method. Therefore, the overall trends in the studied samples reflect genuine trends rather than analytical artefacts.

The $\delta^{34}S_{CRS}$ of the topmost sediment are -9.7‰, -19.4‰, and -32.4‰ in stations SLM23-01, SLM23-04, and SLM23-10, respectively. The $\delta^{34}S$ value of seawater sulfate is considered to be very invariable in today's oceans, around +21‰ (Jørgensen, 2021). Ikonen et al. (2022) has reported $\delta^{34}S$ values around 21–22‰ in the coastal bottom waters of the Gulf of Finland. Therefore, it is reasonable to believe that the isotopic composition of seawater sulfate is around +21‰ in the stations of this study as well. This means that the apparent fractionations ($\varepsilon_{\text{seawater sulfate – pyrite}}$), as sulfate is reduced to sulfide and retained as pyrite in sediments, based on equation 5 (page 13) are 30.7‰ at SLM23-01, 40.5‰ at SLM23-04, and 53.4‰ at SLM23-10. This is a significant variability considering similar sediment properties and environmental conditions (temperature, salinity) in all stations.

This variability could be a result of either a difference in microbial fractionations during sulfate reduction and/or the isotope distillation effect, which depends on the openness of the system (Fike et al., 2015). Although disproportionation possibly influences the isotopic signals, I have discarded the role of disproportionation from this discussion because this effect is difficult to tease apart from other processes (Jørgensen et al., 2019a) and the observed extent of fractionation (<66‰) does not necessarily require disproportionation (Sim et al., 2011). Additionally, our data (larger fractionations in more oxygen-depleted environments) contradict the predicted effect of repeated oxidation and reduction cycles producing high ^{34}S depletions. This indicates the isotopic signal from these cycles has been overwritten by other processes.

Microbial fractionations are contingent on sulfate concentrations and cell-specific sulfate reduction rate, which in turn relates to the availability of labile organic matter (Fike et al., 2015). All coring locations were below the halocline (Estonian Marine Institute, 2023), which means the sulfate concentrations in the overlying seawater would be very similar. This suggests that sulfate concentrations likely do not contribute to the variability in fractionations.

Across the data, no strong correlations between $\delta^{34}S_{CRS}$ and other studied chemical or mineralogical data were found. There is a weak negative correlation between $\delta^{34}S_{CRS}$ and organic matter content (figure 16A), which could simply be a result of their independent depth-related changes (mass-balance effect for isotopes and degradation for organic matter).

There is a strong negative correlation when only studying the upper 0–2 cm of the sediment (figure 16B), where isotopic compositions should best estimate the initial fractionations during microbial sulfate reduction (Jørgensen et al., 2019a). This is counterintuitive because larger electron donor availability should yield faster cell-specific sulfate reduction rates and smaller fractionations (Fike et al., 2015). Therefore, organic matter availability might not straightforwardly control the isotopic fractionation in surface sediments and other contributing factors must be considered.

As explained before, the high organic matter concentrations are likely a result of low metabolic activity in the sediments. Lower sulfate reduction rates could also explain higher fractionations in the western stations. To support that idea, pore water chemistry should also be analysed in two westernmost stations. According to the sulfate profile in Roopõld (2023), there are indications of high sulfate reduction rates in the easternmost station. However, this study cannot explain what could drive the possibly low sulfate reduction rates in the western stations, because sulfate-reducing microorganisms should thrive in anoxic, organic matter rich environments present in these stations (Jørgensen et al., 2019a).

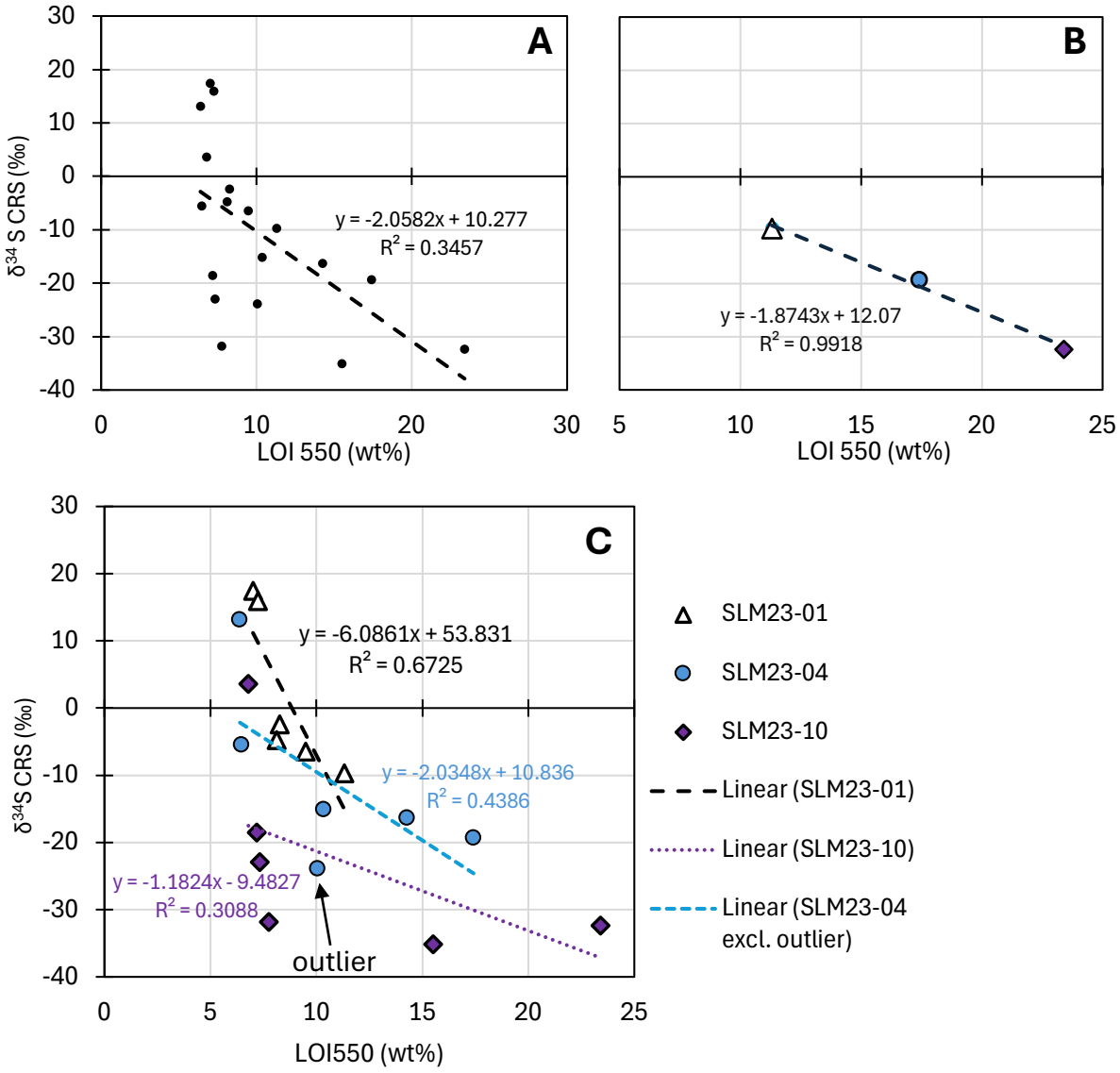

Figure 16. Relation between $\delta^{34}S_{CRS}$ and organic matter concentration (LOI 550) across the data (A, C) and in the uppermost (1–2 cm deep) sediment in the studied stations (B). In C, the outlier (SLM23-04 18 cm) has been removed from the trendline estimation.

Most of the studies analysing the environmental effects on microbial fractionations have been conducted in laboratory conditions (e.g., Canfield, 2001b; Habicht & Canfield, 2001; Harrison & Thode, 1958; Sim et al., 2012). Halevy et al. (2023) have proposed that in natural environments, microbial fractionations always reach the maximum extent because the sulfate reduction rates are considerably lower than in experimental studies. This means that the extent of microbial fractionation becomes secondary, and the isotopic signatures in reduced sulfur species reflect varying degrees of isotope distillation driven by differences in diffusion limitations.

The role of isotope distillation can be discussed through other differences between the stations that could impact the extent of fractionation. These are water depth and sedimentation rate. According to the data collected in this study, larger fractionations occur in deeper waters. Similar variabilities in fractionations have been observed in the Black Sea, where pyrite exhibited $\delta^{34}S$ values from -6‰ to -46‰ moving deeper along the shelf (Wijsman et al., 2001). Additionally, Lein (1983) found that in the Baltic Sea, $\delta^{34}S_{pyrite}$ values in the surface sediments of shallow water stations (<76 m) were higher (-12.8‰ to +6.3‰) than in deep water (>110 m) stations (-18‰ to -26‰).

The water depth and distance from shore are directly related to sediment accumulation rates, and in the case of the Baltic Sea and the Black Sea, also bottom water oxygenation. These are the factors that influence the openness of the system. In a closed or semi-closed system, the apparent fractionation in the surface sediment is smaller because the sulfate pool and produced sulfide gets quickly enriched in ^{34}S. In an open system, the inflow of sulfate with original +21‰ S isotopic composition is high, therefore, the produced sulfide is not enriched in ^{34}S (Claypool, 2004). This indicates that the easternmost and shallowest station, with the smallest apparent fractionation, experiences a more closed system diagenesis. The openness increases with water depth, allowing for higher fractionations in the western stations.

Higher sediment accumulation rate creates a more closed environment by limiting exchange between pore waters and overlying seawater, thereby restricting sulfate diffusion into and out of the sediments. In contrast, a low sedimentation rate allows more time for the diffusion of seawater sulfate into the deeper sediment. Data from Liira et al. (2024) shows that between stations SLM23-04 and SLM23-10, the former experienced higher sedimentation rates. The rate in SLM23-01, although not analysed, is expected to be even higher due to proximity to the coastline. The sedimentation rates could then possibly explain the different $\delta^{34}S$ values seen in the surface sediments.

Oxygenation of the bottom waters might also factor in. Although it is usually reasoned that low-oxygen conditions reduce openness by hindering bio-irrigation and reoxidation of sulfides (e.g., Wijsman et al., 2001), the data of this study suggest otherwise. More oxygen-depleted environments produce higher fractionations, implying a more open behaviour. This can be explained by Fe-sulfide production in the water column. In anoxic conditions, sulfide production may already start in the anoxic water column, creating euxinic conditions. If

reactive Fe is present, Fe-sulfides may start to form in the water column (Rickard & Luther, 2007). In the water column, the system is considerably more open than in the sediment. Therefore, the thicker the layer of anoxic water mass, the larger the depletion in ^{34}S should be seen in bulk sediments. In SLM23-10, this pathway is supported by the unusually high pyrite concentrations (figure 10) coupled to high apparent fractionations (figure 14) at the sediment surface.

Additionally, reactive iron availability can play a huge role in $\delta^{34}S$ values. For example Sim et al. (2012) found that iron deficiency led to higher microbial fractionations. Additionally, reactive iron influences the system's openness with respect to H_2S. When reactive iron availability is high, the produced H_2S is more likely to be fixed into FeS and pyrite in the same sediment horizon (Halevy et al., 2023; Pasquier et al., 2021). Analysing the effect of iron in the studied stations requires estimations of reactive iron availability (using chemical iron extractions).

The CRS (pyrite sulfur) gets progressively more enriched in ^{34}S with depth in all stations. This is the expected isotope distillation effect: as sulfate-reducing microorganisms discriminate against ^{34}S, the remaining sulfate pool gets progressively more enriched in ^{34}S and, so does the sulfide produced from it (Fike et al., 2015). The ^{34}S enrichment with depth also suggests that pyrite continues to form in deeper sediment. This is different from observations from the Bornholm basin in the Baltic Sea, where the $\delta^{34}S_{CRS}$ profile stays consistently at low values, implying that a large majority of the pyrite forms near the sediment surface (J. Liu et al., 2020).

When plotting $\delta^{34}S_{CRS}$ results against pyrite concentrations (figure 17) and organic matter concentrations (figure 16C), only station SLM23-01 shows a clear correlation. The higher the pyrite concentrations and the lower the organic matter concentrations, the larger the $\delta^{34}S_{CRS}$. This is a clear indication of isotope distillation because the more organic matter is degraded and pyrite produced, the more enriched in ^{34}S the pyrite becomes. This relation is weaker in SLM23-04. The $\delta^{34}S_{CRS}$ signals in the westernmost station, SLM23-10, do not relate to organic matter concentrations or pyrite concentrations in any respect. This observation also suggests that station SLM23-01 experiences a steady-state semi-closed system diagenesis. Westward, the system becomes gradually more open and additionally experiences more environmental alterations.

In core SLM23-04, a sharp increase in pyrite concentrations at ~18 cm occurs alongside a drop in $\delta^{34}S_{CRS}$ values, which deviates from the overall increasing trend by about 10‰. This indicates that a large majority of the pyrite in that horizon probably formed close to the sediment surface. Due to the large quantity of pyrite in that front, the additional pyrite forming at depth does not have such an effect on the bulk isotopic composition as it does in other sediment horizons.

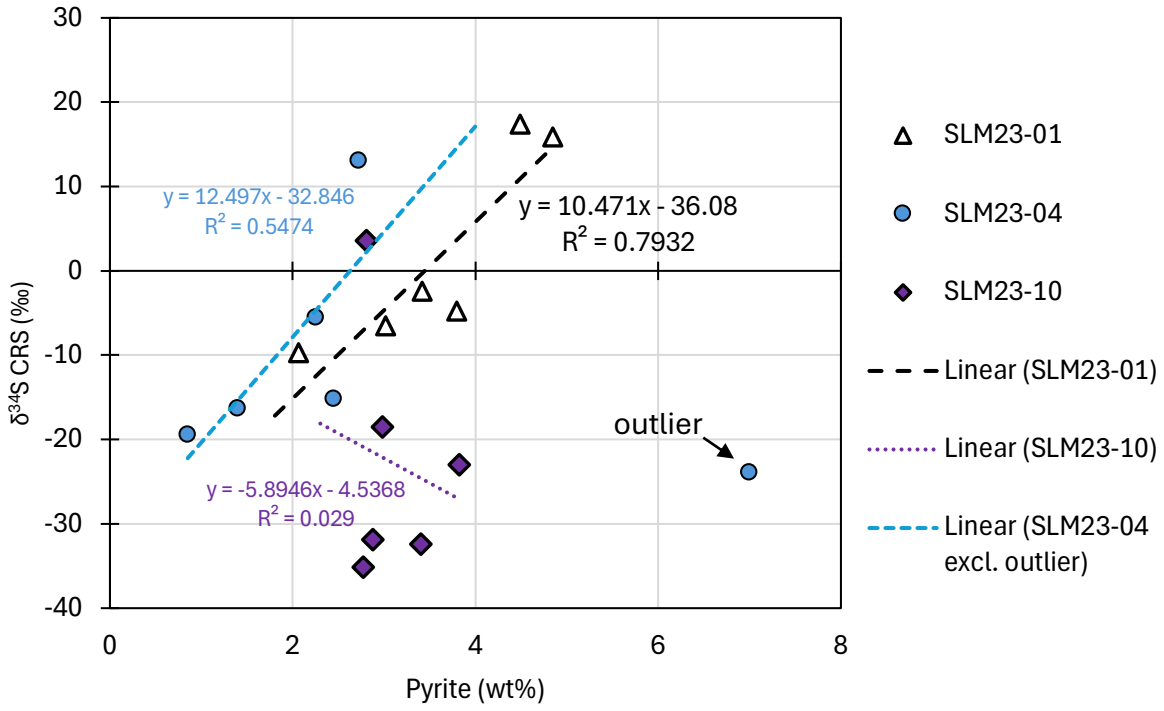

Figure 17. $\delta^{34}S$ of CRS (‰) plotted against pyrite concentrations. The outlier (SLM23-04 at 18 cm) has been removed from the trendline estimation.

One also must consider the possibility of non-steady state processes influencing the depth profile of $\delta^{34}S_{CRS}$. The gradual depth-wise enrichment in ^{34}S might partly be a function of the system getting increasingly open over time, for example, due to the expanding anoxia in the Baltic Sea (Carstensen et al., 2014).

AVS isotope composition

It is usually assumed that the isotopic fractionation during FeS conversion to pyrite is minimal (Jørgensen, 1979). Therefore, the isotopic composition of pyrite sulfur should be the same as the FeS it formed from.

While AVS has a relatively similar isotopic composition to CRS in SLM23-01, there is a clear discrepancy between those species in SLM23-04 and SLM23-10. In these stations, AVS is more enriched in ^{34}S at the sediment surface, but while CRS gets gradually more enriched in ^{34}S with depth, the AVS isotope signal does not significantly change. AVS concentrations in the sediments are considerably lower than CRS concentrations. Due to high solubility, FeS is a more mobile species, and since pyrite forms from dissolved FeS, the transformation from solid FeS to pyrite is not straightforward and is subject to diffusion (Rickard, 2012).

Unlike CRS, the isotopic composition of AVS did not change considerably with depth. This might indicate that FeS forms close to the sediment-water interface, rather than in deeper sediment layers. The AVS that occurs in deeper horizons is a remnant that has not oxidized or transformed into pyrite. Although AVS was not reliably quantified in this study, it has been noted before that AVS tends to experience decreasing concentrations moving from surface to deeper sediments (Rickard, 2012).

Isotope distillation can explain why $\delta^{34}S_{AVS}$ is larger than $\delta^{34}S_{CRS}$ seen in stations SLM23-04 and SLM23-10, assuming that FeS, as an intermediate species in pyrite formation, originally forms later/deeper than most of the pyrite occurring at the same depth. The fact that in SLM23-01, which experiences a more closed system diagenesis, $\delta^{34}S_{AVS}$ was in the same range as $\delta^{34}S_{CRS}$ tells us that when diffusion is limited, FeS and pyrite form at the same depth.

To analyse the environmental effects on $\delta^{34}S_{pyrite}$ further, pore water data (chemistry and isotopic signals of S) should be collected alongside the sediment solid phase. Additionally, concentrations and isotopic signals of organic carbon and nitrogen could cast light on the lability of the organic matter in the sediments. Data about oxygen concentrations in the bottom water would be invaluable for analysing its role in the sulfur cycle. Iron speciation (chemical iron extraction) is useful in determining the role of reactive iron availability. Finally, it would be interesting to analyse the isotopic signals from single pyrite framboids. This could help evaluate the effect of isotope dilution on the $\delta^{34}S_{pyrite}$ of bulk sediments.

6. Conclusions

This thesis aimed to (1) set up and validate an extraction line for AVS and CRS at the University of Tartu and (2) investigate the sulfur cycle in the Estonian Baltic Sea sediments by examining both spatial and vertical variations in mineralogical, chemical, and sulfur isotope compositions.

The development of the extraction line for AVS and CRS at the University of Tartu was successful, despite the need for further refinements to tackle limitations in gas flow stability and AVS and CRS recovery. The analytical uncertainty is considerably lower than the variability in natural sediments and sedimentary rocks and is therefore an effective and reliable method for analysing these materials.

This study provides new insights into the sulfur cycle and its influencing factors in the Baltic Sea sediments. The results overall support the central hypothesis that the depositional environment, particularly water depth, sedimentation rate, and bottom water redox state, influences the isotopic signals of reduced sulfur species.

1. Even seemingly similar sediment properties (organic-rich silty mud) and sedimentation environments (salinity, temperature) can produce distinct sulfur isotopic signals. This study proposes that this is caused by a difference in system openness brought upon by variations in sedimentation rates and bottom water oxygenation.

    - Stations with higher sedimentation rates and shallower depths exhibit more closed-system behaviour, resulting in lower apparent fractionation, whereas deeper, more distal sites show greater fractionations, indicative of more open-system conditions.

    - Isotopically light pyrites in deeper sites may be a result of pyrite formation in the water column due to euxinic conditions.

2. Organic matter concentrations proved to be an unreliable proxy for estimating isotope fractionations in the surface sediments of the studied oxygen-depleted sites.

3. Pyrite formation is present at the sediment-water interface and continues in deeper sediments, producing pyrite that gradually enriches in ^{34}S with depth.

4. The depth profiles of AVS considerably differ from the CRS profiles in the distal sites, with more open-system conditions. In the easternmost sites with a more closed system behaviour, the profiles are alike.

5. Small changes in the sediment properties (i.e., concentration of quartz) can influence the isotopic signals of sulfur.

6. The presence of authigenic framboids associated with organic substances supports the role of localized microenvironments in pyrite formation.

Overall, this work highlights the complexity of sulfur cycling in marine sediments and underscores the importance of integrating mineralogical and environmental data to interpret isotopic signals. Future studies should aim to include pore water chemistry, reactive iron speciation, and deeper sediment profiles to further unravel the controls on sulfur isotope fractionation and its implications for past and present marine redox conditions.

Läänemere merepõhja pindmiste setete väävliringest väävli isotoopsignaalide põhjal

Krete Roopõld

Kokkuvõte

Käesoleva magistritöö eesmärk oli (1) üles seada ja valideerida Tartu Ülikoolis laboratoorne ekstraheermisliin happes lahustuva sulfiidi (AVS) ja kroomiga redutseeritava väävli (CRS) eraldamiseks ning (2) uurida väävliringet Eesti mereala pindmistes setetes erinevate väävlivormide ning nende isotoopsignaalide põhjal. Esitati hüpotees, et redutseeritud väävli isotoopsignaal sõltub settimiskeskkonna tingimustest, seal hulgas veesügavusest, settimiskiirusest ning orgaanilise ainese kättesaadavusest.

Ekstraheermisliini üles seadmine oli edukas, kuid gaasivoolu parema stabiilsuse saavutamiseks ja kvantitatiivseks AVS-i ja CRS-i eraldamiseks oleks vaja teha liinile täiendavaid teste ja parandusi. Sellegipoolest on antud meetodiga eraldatud väävlifraktsioonide isotoopkoostise varieeruvus oluliselt väiksem kui looduslikel setetel ja settekivimitel, mistõttu on tegemist tõhusa meetodiga nende materjalide analüüsimiseks.

Töös uuriti meresetete keemiat kolmest jaamast, mis paiknesid ida-lääne-suunalisel profiilil Soome lahe suudmest Läänemere põhjaosa keskaladeni. Veesügavused jaamades idast lääne suunas olid vastavalt 100 m, 107 m ja 166 m ning setteläbilõigete paksused 55 cm, 52 cm ja 43 cm. Settetüübiks oli kõikides jaamades aleuriitne orgaanikarikas muda. Setteproovidest eraldati AVS (~FeS) ja CRS (~püriit FeS_2) fraktsioonid ning analüüsiti nende väävli isotoopkoostist. Tulemused kõrvutati mineraloogiliste ja keemiliste andmetega. Lisaks uuriti skaneeriva elektronmikroskoobiga püriidiframboidide esinemist.

Töö tulemused üldjoontes toetavad hüpoteesi, et settekeskkond mõjutab redutseeritud väävliühendite isotoopsignaale. Leiti, et isegi näiliselt sarnaste omadustega setetes võivad redutseeritud väävli isotoopsisaldused suuresti erineda. Antud töös tuletatakse, et selle põhjuseks on erinevused süsteemi avatusest, mis tulenevad settimiskiiruse ning vee põhjakihi hapnikusisalduse varieeruvustest. Suurem settimiskiirus rannikulähedasematel aladel põhjustab süsteemi suletumat käitumust, mille tulemuseks on väiksemad näivad isotoopide fraktsioneerumised. Sügavamates ja rannikust kaugemates jaamades esinevate püriitide

isotoopsuhted on negatiivsemad, mille põhjuseks on väiksem settimiskiirus. Lisaks on võimalik, et nendes jaamades on osa püriidist tekkinud veesambas euksiinilistes tingimustes. Orgaanilise ainese sisalduse ja S-isotoopide väärtuste omavahelised suhted ei osutunud antud andmestikus ootuspäraseks hapnikuvaeste tingimuste tõttu.

Töö tulemused näitavad, et püriidi tekkimine toimub juba settepinna lähedal ning jätkub sügavamates kihtides, mille tulemusena püriit rikastub järk-järgult raskematest isotoopidest. Väiksed erinevused sette omadustes (nt kvartsi sisalduses) võivad märkimisväärselt mõjutada väävli isotoopsignaale.

Püriidiframboidide esinemine kinnitas, et püriit setetes on autigeenne. Avastati, et suur osa settes olevatest framboididest on seotud orgaaniliste kilede jm elutekkeliste substraatidega. Selline tähelepanek toetab difusiooni limiteerivate ja orgaanikarikaste mikrokeskkondade olulist rolli püriidi tekkes.

Kokkuvõttes toob antud magistritöö esile väävliringe keerukuse meresetetes ning rõhutab keskkonnaalase ja geokeemilise konteksti olulisust isotoopsignaalide tõlgendamisel. Tulevasted uuringud võiksid hõlmata ka poorivee keemiat, reaktiivse raua sisalduse määramist ning sügavamaid setteprofiile, et paremini mõista väävli isotoopfraktsioneerumist kontrollivaid faktoreid ning nende tähendust nii tänapäevases kontekstis kui ka geoloogilises ajaloos.

Acknowledgements

The author of this thesis would like to express gratitude to Dr. Kärt Paiste and Dr. Martin Liira for their dedicated supervision. Special thanks are extended to those who provided invaluable support with laboratory analyses: Holar Sepp for conducting the IRMS analysis, Jaan Aruväli for doing the XRD analysis, Peeter Somelar for XRD diffractogram modelling, Marian Külaviir for help with SEM imaging, and Siim Salmar and Anton Mastitski from the University of Tartu Institute of Chemistry for assistance with freeze-drying. Additionally, the author would like to thank Prof. Kalle Kirsimäe, Prof. David Fike, and Dr. Aivo Lepland for valuable insights. This work was supported by the Estonian Research Council grant PSG944.

References

Björck, S. (1995). A Review of the History of the Baltic Sea, 13.0-8.0 ka BP. *Quaternary Lnternational*, *27*, 19–40. https://doi.org/10.1016/1040-6182(94)00057-C

Böttcher, M. E., Smock, A. M., & Cypionka, H. (1998). Sulfur isotope fractionation during experimental precipitation of iron(II) and manganese(II) sulfide at room temperature. *Chemical Geology*, *146*(3), 127–134. https://doi.org/10.1016/S0009-2541(98)00004-7

Canfield, D. E. (2001a). Biogeochemistry of Sulfur Isotopes. *Reviews in Mineralogy and Geochemistry*, *43*(1), 607–636. https://doi.org/10.2138/gsrmg.43.1.607

Canfield, D. E. (2001b). Isotope fractionation by natural populations of sulfate-reducing bacteria. *Geochimica et Cosmochimica Acta*, *65*(7), 1117–1124. https://doi.org/10.1016/S0016-7037(00)00584-6

Canfield, D. E., Erik Kristensen, & Bo Thamdrup. (2005). The Sulfur Cycle. In D. E. Canfield, E. Kristensen, & B. Thamdrup (Eds.), *Advances in Marine Biology* (Vol. 48, pp. 313–381). Academic Press. https://doi.org/10.1016/S0065-2881(05)48009-8

Canfield, D. E., Raiswell, R., Westrich, J. T., Reaves, C. M., & Berner, R. A. (1986). The use of chromium reduction in the analysis of reduced inorganic sulfur in sediments and shales. *Chemical Geology*, *54*(1–2), 149–155. https://doi.org/10.1016/0009-2541(86)90078-1

Canfield, D. E., & Teske, A. (1996). Late Proterozoic rise in atmospheric oxygen concentration inferred from phylogenetic and sulphur-isotope studies. *Nature*, *382*(6587), 127–132. https://doi.org/10.1038/382127a0

Canfield, D. E., & Thamdrup, B. (1994). The Production of 34S-Depleted Sulfide During Bacterial Disproportionation of Elemental Sulfur. *Science*, *266*(5193), 1973–1975. https://doi.org/10.1126/science.11540246

Canfield, D. E., Thamdrup, B., & Fleischer, S. (1998). Isotope fractionation and sulfur metabolism by pure and enrichment cultures of elemental sulfur disproportionating bacteria. *Limnology and Oceanography*, *43*(2), 253–264. https://doi.org/10.4319/lo.1998.43.2.0253

Carstensen, J., Andersen, J. H., Gustafsson, B. G., & Conley, D. J. (2014). Deoxygenation of the Baltic Sea during the last century. *Proceedings of the National Academy of Sciences*, *111*(15), 5628–5633. https://doi.org/10.1073/pnas.1323156111

Claypool, G. E. (2004). Ventilation of marine sediments indicated by depth profiles of pore water sulfate and δ34S. In R. J. Hill, J. Leventhal, Z. Aizenshtat, M. J. Baedecker, G. Claypool, R. Eganhouse, M. Goldhaber, & K. Peters (Eds.), *The Geochemical Society Special Publications* (Vol. 9, pp. 59–65). Elsevier. https://doi.org/10.1016/S1873-9881(04)80007-5

Conley, D. J., Björck, S., Bonsdorff, E., Carstensen, J., Destouni, G., Gustafsson, B. G., Hietanen, S., Kortekaas, M., Kuosa, H., Markus Meier, H. E., Müller-Karulis, B., Nordberg, K., Norkko, A., Nürnberg, G., Pitkänen, H., Rabalais, N. N., Rosenberg, R., Savchuk, O. P., Slomp, C. P., … Zillén, L. (2009). Hypoxia-Related Processes in the Baltic Sea. *Environmental Science & Technology*, *43*(10), 3412–3420. https://doi.org/10.1021/es802762a

D'Hondt, S., Inagaki, F., Zarikian, C. A., Abrams, L. J., Dubois, N., Engelhardt, T., Evans, H., Ferdelman, T., Gribsholt, B., Harris, R. N., Hoppie, B. W., Hyun, J.-H., Kallmeyer, J., Kim, J., Lynch, J. E., McKinley, C. C., Mitsunobu, S., Morono, Y., Murray, R. W., … Ziebis, W. (2015). Presence of oxygen and aerobic communities from sea floor to basement in deep-sea sediments. *Nature Geoscience*, *8*(4), 299–304. https://doi.org/10.1038/ngeo2387

Egger, M., Riedinger, N., Mogollón, J. M., & Jørgensen, B. B. (2018). Global diffusive fluxes of methane in marine sediments. *Nature Geoscience*, *11*(6), 421–425. https://doi.org/10.1038/s41561-018-0122-8

EMODnet. (2024). *Digital Bathymetry* [Map]. European Commission. Accessed: 01.03.2025, https://emodnet.ec.europa.eu/en/bathymetry

Estonian Marine Institute. (2023). *Avamere seire 2022. A.* [Dataset]. Estonian Environment Agency's environmental monitoring database KESE. Accessed: 25.04.2025, https://kese.envir.ee

Fike, D. A., Bradley, A. S., & Rose, C. V. (2015). Rethinking the Ancient Sulfur Cycle. *Annual Review of Earth and Planetary Sciences*, *43*(1), 593–622. https://doi.org/10.1146/annurev-earth-060313-054802

Froelich, P. N., Klinkhammer, G. P., Bender, M. L., Luedtke, N. A., Heath, G. R., Cullen, D., Dauphin, P., Hammond, D., Hartman, B., & Maynard, V. (1979). Early oxidation of organic matter in pelagic sediments of the eastern equatorial Atlantic: Suboxic diagenesis. *Geochimica et Cosmochimica Acta*, *43*(7), 1075–1090. https://doi.org/10.1016/0016-7037(79)90095-4

Habicht, K. S., & Canfield, D. E. (2001). Isotope fractionation by sulfate-reducing natural populations and the isotopic composition of sulfide in marine sediments. *Geology*, *29*(6), 555–558. https://doi.org/10.1130/0091-7613(2001)029<0555:IFBSRN>2.0.CO;2

Habicht, K. S., Gade, M., Thamdrup, B., Berg, P., & Canfield, D. E. (2002). Calibration of Sulfate Levels in the Archean Ocean. *Science*, *298*(5602), 2372–2374. https://doi.org/10.1126/science.1078265

Halevy, I., Fike, D. A., Pasquier, V., Bryant, R. N., Wenk, C. B., Turchyn, A. V., Johnston, D. T., & Claypool, G. E. (2023). Sedimentary parameters control the sulfur isotope composition of marine pyrite. *Science*, *382*(6673), 946–951. https://doi.org/10.1126/science.adh1215

Hansson, M., & Viktorsson, L. (2021). Oxygen Survey in the Baltic Sea 2021—Extent of Anoxia and Hypoxia, 1960-2021 | SMHI. *Report Oceanography*, *72*. https://www.smhi.se/publikationer/oxygen-survey-in-the-baltic-sea-2021-extent-of-anoxia-and-hypoxia-1960-2021-1.184040

Harrison, A. G., & Thode, H. G. (1958). Mechanism of the bacterial reduction of sulphate from isotope fractionation studies. *Transactions of the Faraday Society*, *54*(0), 84–92. https://doi.org/10.1039/TF9585400084

Ikonen, J., Hendriksson, N., Luoma, S., Lahaye, Y., & Virtasalo, J. J. (2022). Behavior of Li, S and Sr isotopes in the subterranean estuary and seafloor pockmarks of the Hanko

submarine groundwater discharge site in Finland, northern Baltic Sea. *Applied Geochemistry*, *147*, 105471. https://doi.org/10.1016/j.apgeochem.2022.105471

Jørgensen, B. B. (1979). A theoretical model of the stable sulfur isotope distribution in marine sediments. *Geochimica et Cosmochimica Acta*, *43*(3), 363–374. https://doi.org/10.1016/0016-7037(79)90201-1

Jørgensen, B. B. (1982). Mineralization of organic matter in the sea bed—The role of sulphate reduction. *Nature*, *296*(5858), 643–645. https://doi.org/10.1038/296643a0

Jørgensen, B. B. (2021). Sulfur Biogeochemical Cycle of Marine Sediments. *Geochemical Perspectives*, 145–307. https://doi.org/10.7185/geochempersp.10.2

Jørgensen, B. B., & Bak, F. (1991). Pathways and Microbiology of Thiosulfate Transformations and Sulfate Reduction in a Marine Sediment (Kattegat, Denmark). *Applied and Environmental Microbiology*, *57*(3), 847–856. https://doi.org/10.1128/aem.57.3.847-856.1991

Jørgensen, B. B., Beulig, F., Egger, M., Petro, C., Scholze, C., & Røy, H. (2019b). Organoclastic sulfate reduction in the sulfate-methane transition of marine sediments. *Geochimica et Cosmochimica Acta*, *254*, 231–245. https://doi.org/10.1016/j.gca.2019.03.016

Jørgensen, B. B., Böttcher, M. E., Lüschen, H., Neretin, L. N., & Volkov, I. I. (2004). Anaerobic methane oxidation and a deep H2S sink generate isotopically heavy sulfides in Black Sea sediments 1. *Geochimica et Cosmochimica Acta*, *68*(9), 2095–2118. https://doi.org/10.1016/j.gca.2003.07.017

Jørgensen, B. B., Egger, M., & Canfield, D. E. (2024). Sulfate distribution and sulfate reduction in global marine sediments. *Geochimica et Cosmochimica Acta*, *364*, 79–88. https://doi.org/10.1016/j.gca.2023.11.015

Jørgensen, B. B., Findlay, A. J., & Pellerin, A. (2019a). The Biogeochemical Sulfur Cycle of Marine Sediments. *Frontiers in Microbiology*, *10*, 849. https://doi.org/10.3389/fmicb.2019.00849

Jørgensen, B. B., & Kasten, S. (2006). Sulfur Cycling and Methane Oxidation. In H. D. Schulz & M. Zabel (Eds.), *Marine Geochemistry* (pp. 271–309). Springer. https://doi.org/10.1007/3-540-32144-6_8

Lahtvee, D. (2023). *Uranium and molybdenum contents of the bottom sediments of the Estonian sea area and their role in explaining the redox conditions of the seafloor* [Bachelor's thesis, University of Tartu] (in Estonian). https://dspace.ut.ee/items/b6268b0a-2360-49fd-aa0a-8162d2484e4a

Leavitt, W. D., Halevy, I., Bradley, A. S., & Johnston, D. T. (2013). Influence of sulfate reduction rates on the Phanerozoic sulfur isotope record. *Proceedings of the National Academy of Sciences*, *110*(28), 11244–11249. https://doi.org/10.1073/pnas.1218874110

Lein, A. Yu. (1983). Biogeochemistry of the Anaerobic Diagenesis of Recent Baltic Sea Sediments. *Ecological Bulletins*, *35*, 441–461.

Liira, M., Ausmeel, M., Suuroja, S., Veski, A., & Tuuling, I. (2024). *Eesti Läänemere avaosa põhjasetete keskkonnaseisundi hindamise metoodika rakendamine ja alusandmete kogumine* (in Estonian). Eesti Geoloogiateenistus. https://fond.egt.ee/fond/egf/9919

Liu, J., Pellerin, A., Antler, G., Kasten, S., Findlay, A. J., Dohrmann, I., Røy, H., Turchyn, A. V., & Jørgensen, B. B. (2020). Early diagenesis of iron and sulfur in Bornholm Basin sediments: The role of near-surface pyrite formation. *Geochimica et Cosmochimica Acta*, *284*, 43–60. https://doi.org/10.1016/j.gca.2020.06.003

Liu, X., Fike, D., Li, A., Dong, J., Xu, F., Zhuang, G., Rendle-Bühring, R., & Wan, S. (2019). Pyrite sulfur isotopes constrained by sedimentation rates: Evidence from sediments on the East China Sea inner shelf since the late Pleistocene. *Chemical Geology*, *505*, 66–75. https://doi.org/10.1016/j.chemgeo.2018.12.014

Luther, G. W. (2005). Acid volatile sulfide—A comment. *Marine Chemistry*, *97*(3), 198–205. https://doi.org/10.1016/j.marchem.2005.08.001

Masterson, A. L., Alperin, M. J., Arnold, G. L., Berelson, W. M., Jørgensen, B. B., Røy, H., & Johnston, D. T. (2022). Understanding the isotopic composition of sedimentary sulfide:

A multiple sulfur isotope diagenetic model for Aarhus Bay. *American Journal of Science*, *322*(1), 1–27. https://doi.org/10.2475/01.2022.01

Niewöhner, C., Hensen, C., Kasten, S., Zabel, M., & Schulz, H. D. (1998). Deep Sulfate Reduction Completely Mediated by Anaerobic Methane Oxidation in Sediments of the Upwelling Area off Namibia. *Geochimica et Cosmochimica Acta*, *62*(3), 455–464. https://doi.org/10.1016/S0016-7037(98)00055-6

Pasquier, V., Bryant, R. N., Fike, D. A., & Halevy, I. (2021). Strong local, not global, controls on marine pyrite sulfur isotopes. *Science Advances*, *7*(9), eabb7403. https://doi.org/10.1126/sciadv.abb7403

Pellerin, A., Gilad, A., Holm, S., Findlay, A., Crockford, P., Turchyn, A., Jørgensen, B., & Finster, K. (2019). Large sulfur isotope fractionation by bacterial sulfide oxidation. *Science Advances*, *5*. https://doi.org/10.1126/sciadv.aaw1480

Piker, L., Schmaljohann, R., & Imhoff, J. (1998). Dissimilatory sulfate reduction and methane production in Gotland Deep sediments (Baltic Sea) during a transition period from oxic to anoxic bottom water (1993-1996). *Aquatic Microbial Ecology*, *14*, 183–193. https://doi.org/10.3354/ame014183

Rickard, D. (2012). Chapter 6—Sedimentary Pyrite. In D. Rickard (Ed.), *Developments in Sedimentology* (Vol. 65, pp. 233–285). Elsevier. https://doi.org/10.1016/B978-0-444-52989-3.00006-4

Rickard, D. (2019). How long does it take a pyrite framboid to form? *Earth and Planetary Science Letters*, *513*, 64–68. https://doi.org/10.1016/j.epsl.2019.02.019

Rickard, D., & Luther, G. W. (1997). Kinetics of pyrite formation by the H 2S oxidation of iron (II) monosulfide in aqueous solutions between 25 and 125°C: The mechanism. *Geochimica et Cosmochimica Acta*, *61*, 135–147. https://doi.org/10.1016/S0016-7037(96)00322-5

Rickard, D., & Luther, G. W. (2007). Chemistry of Iron Sulfides. *Chemical Reviews*, *107*(2), 514–562. https://doi.org/10.1021/cr0503658

Rickard, D., & Morse, J. W. (2005). Acid volatile sulfide (AVS). *Marine Chemistry*, *97*(3), 141–197. https://doi.org/10.1016/j.marchem.2005.08.004

Roopõld, K. (2023). *Assessment of porewater geochemistry and potential anaerobic methane oxidation in the bottom sediments of the Gulf of Finland based on porewater sulfate profiles* [Bachelor's thesis, University of Tartu] (in Estonian). https://dspace.ut.ee/items/e81ec395-8793-4b62-9759-88fcdd649e3d

Røy, H., Kallmeyer, J., Adhikari, R. R., Pockalny, R., Jørgensen, B. B., & D'Hondt, S. (2012). Aerobic Microbial Respiration in 86-Million-Year-Old Deep-Sea Red Clay. *Science*, *336*(6083), 922–925. https://doi.org/10.1126/science.1219424

Rullkötter, J. (2006). Organic Matter: The Driving Force for Early Diagenesis. In H. D. Schulz & M. Zabel (Eds.), *Marine Geochemistry* (pp. 125–168). Springer. https://doi.org/10.1007/3-540-32144-6_4

Sardisco, L., Hirani, J., & Pearce, T. J. (2022). *Characterization of the Estonian Metalliferous Shale (EMS-1)* [Certificate of Analysis]. X-Ray Mineral Services Finland.

Schulz, H. D. (2006). Quantification of Early Diagenesis: Dissolved Constituents in Pore Water and Signals in the Solid Phase. In H. D. Schulz & M. Zabel (Eds.), *Marine Geochemistry* (pp. 73–124). Springer. https://doi.org/10.1007/3-540-32144-6_3

Sim, M. S., Bosak, T., & Ono, S. (2011). Large Sulfur Isotope Fractionation Does Not Require Disproportionation. *Science*, *333*(6038), 74–77. https://doi.org/10.1126/science.1205103

Sim, M. S., Ono, S., & Bosak, T. (2012). Effects of Iron and Nitrogen Limitation on Sulfur Isotope Fractionation during Microbial Sulfate Reduction. *Applied and Environmental Microbiology*, *78*(23), 8368–8376. https://doi.org/10.1128/AEM.01842-12

Tuuling, I. (Ed.). (2011). *The Baltic Sea: Geology and geotourism highlights*. NGO GeoGuide Baltoscandia, 2011.

Vairavamurthy, M. A., Orr, W. L., & Manowitz, B. (1995). Geochemical Transformations of Sedimentary Sulfur: An Introduction. In *Geochemical Transformations of Sedimentary*

Sulfur (Vol. 612, pp. 1–14). American Chemical Society. https://doi.org/10.1021/bk-1995-0612.ch001

Wang, Q., & Morse, J. W. (1996). Pyrite formation under conditions approximating those in anoxic sediments I. Pathway and morphology. *Marine Chemistry*, *52*(2), 99–121. https://doi.org/10.1016/0304-4203(95)00082-8

Wijsman, J. W. M., Middelburg, J. J., Herman, P. M. J., Böttcher, M. E., & Heip, C. H. R. (2001). Sulfur and iron speciation in surface sediments along the northwestern margin of the Black Sea. *Marine Chemistry*, *74*(4), 261–278. https://doi.org/10.1016/S0304-4203(01)00019-6

Wilkin, R. T., Barnes, H. L., & Brantley, S. L. (1996). The size distribution of framboidal pyrite in modern sediments: An indicator of redox conditions. *Geochimica et Cosmochimica Acta*, *60*(20), 3897–3912. https://doi.org/10.1016/0016-7037(96)00209-8

Supplementary materials

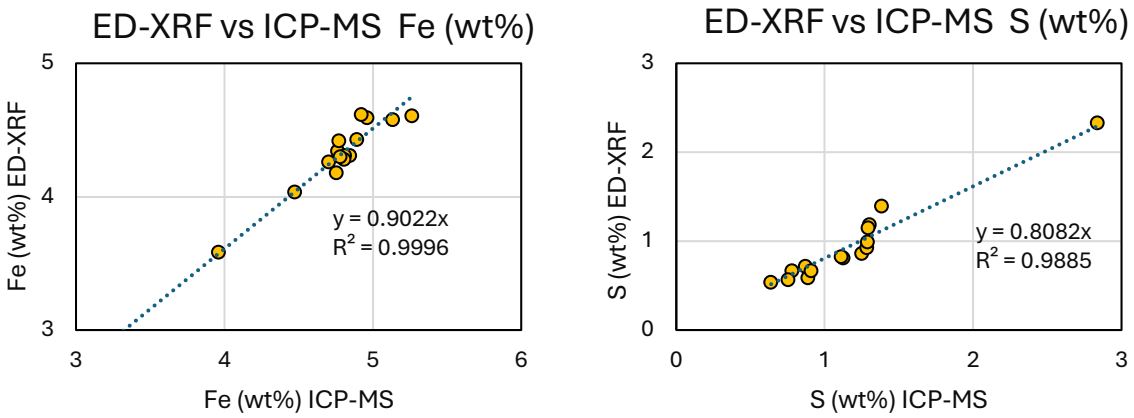

Supplementary figure 1. Correlation graphs for ED-XRF results and ICP-MS results for Fe and S in the sediments at stations SLM23-04 and SLM23-10.

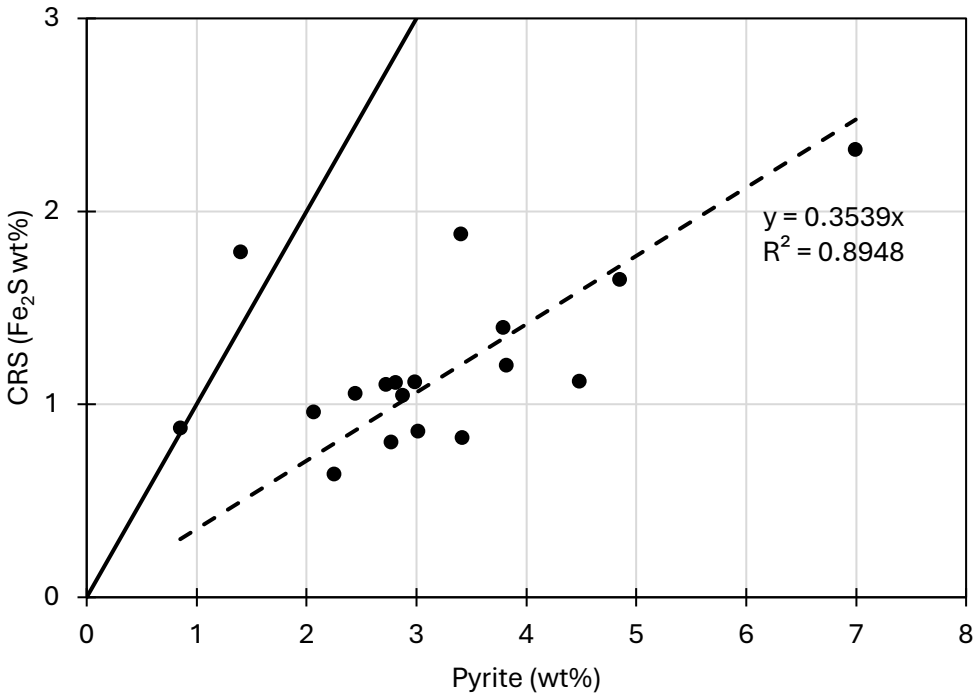

Supplementary figure 2. Relation between recovered CRS (calculated to Fe_2S percentages) and pyrite concentrations in analysed sediments (measured with XRD and normalised with LOI 550). The dotted line is the linear trendline. The solid line shows the ideal relation if all pyrite sulfur were recovered.

Supplementary table 1. Water content and LOI 550°C (organic matter content in dry sediment)

Sample	Depth (up) (cm)	Depth (low) (cm)	Water content (wt%)*	LOI 550 °C (wt%)*
SLM23-01-1	1	3	90.11	11.31
SLM23-01-3	3	5	84.11	10.76
SLM23-01-5	5	7	81.41	9.89
SLM23-01-7	7	9	82.29	9.83
SLM23-01-9	9	12	80.99	9.49
SLM23-01-14	14	16	80.29	9.37
SLM23-01-18	18	20	77.41	8.26
SLM23-01-22	22	24	73.67	9.01
SLM23-01-28	28	30		8.13
SLM23-01-38	38	40	68.66	7.01
SLM23-01-48	48	50	66.08	7.24
SLM23-04-0	0.0	1.1	97.30	18.86
SLM23-04-1	1.1	2.1		17.41
SLM23-04-4	4.2	5.3	90.39	14.27
SLM23-04-7	7.4	8.5	87.15	15.88
SLM23-04-10	10.6	11.7	82.29	10.35
SLM23-04-13	13.8	14.9	78.19	10.08
SLM23-04-16	17.0	18.0	83.47	10.07
SLM23-04-19	20.2	21.2	72.87	8.03
SLM23-04-29	30.8	31.8	65.36	6.48
SLM23-04-45	47.8	48.8	65.04	6.39
SLM23-10-0	0.0	1.0	89.21	23.39
SLM23-10-1	1.0	2.1	84.41	18.31
SLM23-10-4	4.2	5.2	78.58	15.50
SLM23-10-7	7.3	8.4	71.07	8.57
SLM23-10-10	10.5	11.5	68.63	7.75
SLM23-10-13	13.6	14.7	67.96	7.38
SLM23-10-16	16.8	17.8	67.92	7.32
SLM23-10-19	19.9	21.0	71.30	7.28
SLM23-10-29	30.4	31.5	67.42	6.79
SLM23-10-40	42.0	43.0	66.75	7.20

*results for SLM23-04 and SLM23-10 are from Liira et al. (2024)

Supplementary table 2. Sediment mineralogy analysed with X-ray diffraction and normalised to whole sample using LOI 550°C results.

Sample	Pyrite (wt%)	Quartz (wt%)	K-feldspar (wt%)	Plagioclase (wt%)	Mica/illite/I-S (wt%)	Kaolinite (wt%)	Halite (wt%)
SLM23-01-1	2.07	17.52	9.88	10.96	32.97	3.95	5.75
SLM23-01-3	1.81	18.69	12.01	10.74	35.12	3.52	2.71
SLM23-01-5	2.46	17.93	11.92	10.46	35.03	3.82	3.18
SLM23-01-7	2.73	18.30	12.29	10.02	34.87	4.28	2.91
SLM23-01-9	3.01	18.18	11.05	10.59	35.07	4.29	2.92
SLM23-01-14	3.66	18.10	11.80	10.61	34.47	4.39	2.47
SLM23-01-18	3.42	17.92	10.90	10.99	35.75	4.16	2.86
SLM23-01-22	4.31	18.16	9.63	10.55	34.95	4.13	2.57
SLM23-01-28	3.79	16.92	11.56	11.19	36.07	4.81	2.31
SLM23-01-38	4.49	17.66	10.93	11.68	35.88	3.64	1.78
SLM23-01-48	4.85	18.46	9.88	10.72	35.71	4.10	1.68
SLM23-04-1	0.85	13.12	8.77	8.60	21.38	4.77	22.91
SLM23-04-4	1.40	17.24	10.50	11.46	27.13	3.94	8.49
SLM23-04-7	1.38	17.17	10.10	11.65	26.75	3.97	8.03
SLM23-04-10	2.45	18.58	11.24	13.59	30.72	3.08	4.53
SLM23-04-13	4.00	20.17	10.36	11.36	32.52	3.36	3.36
SLM23-04-16	7.00	22.08	9.72	10.27	27.98	3.82	4.18
SLM23-04-19	3.05	19.16	11.76	13.89	31.29	3.98	2.41
SLM23-04-29	2.25	21.22	11.18	12.68	34.94	2.72	1.69
SLM23-04-45	2.73	19.64	11.37	13.16	34.78	3.48	1.50
SLM23-10-0	3.40	16.69	8.19	9.48	25.12	3.24	8.59
SLM23-10-1	2.96	17.33	9.04	9.38	28.99	3.63	6.34
SLM23-10-4	2.77	17.23	9.61	12.21	28.74	4.33	3.64
SLM23-10-7	2.30	17.59	8.93	12.53	37.58	3.04	2.30
SLM23-10-10	2.88	17.35	9.28	12.81	36.66	3.34	2.23
SLM23-10-13	3.35	17.69	9.13	12.67	37.44	2.98	2.42
SLM23-10-16	3.82	17.89	9.78	12.86	34.48	3.63	2.70
SLM23-10-19	3.45	17.52	9.32	12.77	36.63	3.54	2.14
SLM23-10-29	2.81	18.07	9.46	13.11	36.99	3.46	2.06
SLM23-10-40	2.99	18.10	9.42	12.50	36.29	3.92	2.05

Supplementary table 3. Iron (Fe) and sulfur (S) concentrations in dry sediment measured with ED-XRF and ICP-MS.

	ED-XRF		ICP-MS	
Sample	Fe (wt%)	S (wt%)	Fe (mg/kg)*	S (mg/kg)*
SLM23-01-1	3.99	1.14		
SLM23-01-3	3.96	0.84		
SLM23-01-5	4.11	1.02		
SLM23-01-7	4.21	1.08		
SLM23-01-9	4.30	1.13		
SLM23-01-14	4.47	1.20		
SLM23-01-18	4.25	0.96		
SLM23-01-22	4.32	1.36		
SLM23-01-28	4.13	0.96		
SLM23-01-38	4.32	1.19		
SLM23-01-48	4.35	1.11		
SLM23-04-0			24396.0	15611.4
SLM23-04-1			30084.0	14862.5
SLM23-04-4			43732.1	16015.3
SLM23-04-7			45152.1	16113.3
SLM23-04-10	4.18	1.39	47530.9	13861.7
SLM23-04-13	4.03	1.19	44737.7	13038.4
SLM23-04-16	4.60	2.33	52619.0	28386.3
SLM23-04-19	4.31	0.86	48449.7	12527.2
SLM23-04-29	4.34	0.59	47624.3	8866.6
SLM23-04-45	4.31	0.71	48113.1	8707.4
SLM23-10-0			39530.6	14872.8
SLM23-10-1	3.58	1.15	39596.2	12942.2
SLM23-10-4	4.28	0.92	48057.1	12866.3
SLM23-10-7	4.26	0.54	47005.2	6388.1
SLM23-10-10	4.42	0.67	47695.0	7800.0
SLM23-10-13	4.59	0.81	49598.1	11256.0
SLM23-10-16	4.57	0.99	51353.0	12907.9
SLM23-10-19	4.62	0.82	49201.3	11136.3
SLM23-10-29	4.43	0.66	48917.4	9083.0
SLM23-10-40	4.30	0.56	47792.6	7541.2

*from Liira et al. (2024)

Supplementary table 4. Concentrations and sulfur isotopic compositions $\delta^{34}S_{VDCT}$ (‰) of AVS and CRS in the samples.

Sample	Depth (up) (cm)	Depth (low) (cm)	AVS		CRS	
			wt% S	$\delta^{34}S_{VDCT}$ (‰)	wt% S	$\delta^{34}S_{VDCT}$ (‰)
SLM23-01-1	1	3	< 0.01	-11.48	0.51	-9.71
SLM23-01-5	5	7	< 0.01	-7.53		
SLM23-01-9	9	12	< 0.01	-2.18	0.46	-6.49
SLM23-01-9.2	9	12	< 0.01	-3.55		
SLM23-01-18	18	20	< 0.01		0.44	-2.41
SLM23-01-28	28	30	< 0.01	-6.76	0.75	-4.79
SLM22-01-38	38	40	< 0.01		0.60	17.44
SLM223-01-48	48	50	< 0.01		0.88	15.92
SLM23-04-1	0	2.1	< 0.01	-13.29	0.47	-19.38
SLM23-04-4	4.2	5.3	~0.011	-14.44	0.96	-16.33
SLM23-04-10	10.6	11.7	~0.03	-15.83	0.57	-15.14
SLM23-04-16	17.0	18.0	< 0.01		1.24	-23.92
SLM23-04-29	30.8	31.8	< 0.01		0.34	-5.52
SLM23-04-45	47.8	48.8	< 0.01	-15.74	0.59	13.09
SLM23-10-0	0	1.0	< 0.01	-19.63	1.01	-32.38
SLM23-10-4	4.2	5.2	< 0.01	-22.99	0.43	-35.13
SLM23-10-10	10.5	11.5	< 0.01		0.56	-31.83
SLM23-10-16	16.8	17.8	< 0.01		0.64	-22.96
SLM23-10-29	30.4	31.5	< 0.01	-16.98	0.60	3.57
SLM23-10-40	42.0	43.0	< 0.01		0.60	-18.52

Non-exclusive licence to reproduce the thesis and make the thesis public

I, Krete Roopõld,

1. grant the University of Tartu a free permit (non-exclusive licence) to

reproduce, for the purpose of preservation, including for adding to the digital archives of the University of Tartu until the expiry of the term of copyright, my thesis

Insight into the sulfur cycle in the Baltic Sea surface sediments based on sulfur isotope records

supervised by Kärt Paiste and Martin Liira;

2. grant the University of Tartu a permit to make the thesis specified in point 1 available to the public via the web environment of the University of Tartu, including via the digital archives, under the Creative Commons licence CC BY NC ND 4.0, which allows, by giving appropriate credit to the author, to reproduce, distribute the work and communicate it to the public, and prohibits the creation of derivative works and any commercial use of the work until the expiry of the term of copyright;

3. am aware of the fact that the author retains the rights specified in points 1 and 2;

4. confirm that granting the non-exclusive licence does not infringe other persons' intellectual property rights or rights arising from the personal data protection legislation.

Krete Roopõld
26/05/2025